

AD-A055 640

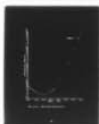
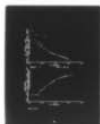
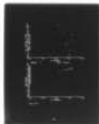
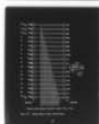
AIR FORCE INST OF TECH WRIGHT-PATTERSON AFB OHIO SCH--ETC F/G 11/2
MAGNETORESISTANCE AND HALL MEASUREMENT OF ULTRA-PURE SILICON.(U)
DEC 77 R G SCHWEIN

UNCLASSIFIED

AFIT/GE0/PH/78-1

NL

1 OF 1
ADA
055640



END
DATE
FILMED
8-78
DDC

FOR FURTHER TRAN

2

(1)

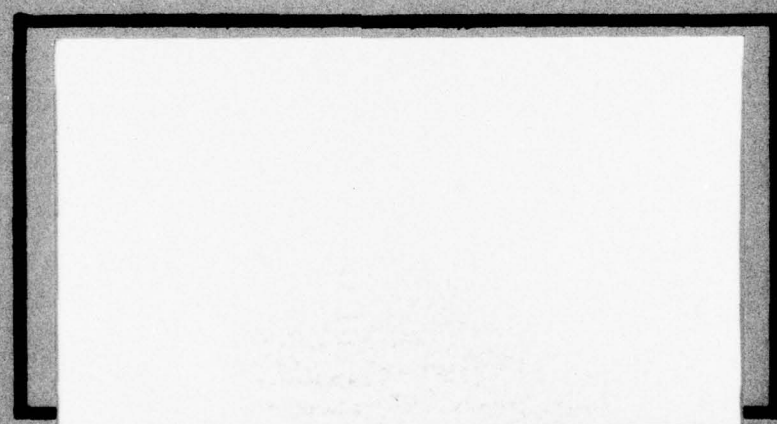


DDC
JUN 21 1988
AF

AD NO. _____
DDC FILE COPY

AD A055640

*See back page
for 1473*



UNITED STATES AIR FORCE
AIR UNIVERSITY
AIR FORCE INSTITUTE OF TECHNOLOGY
Wright-Patterson Air Force Base, Ohio

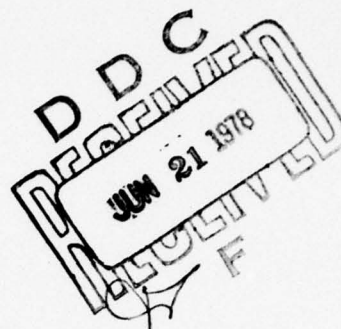
78 06 15 072

This document has been approved
for public release and sale; its
distribution is unlimited.

AD No. _____
DDC FILE COPY

AD A 055640

(1)



MAGNETORESISTANCE AND HALL
MEASUREMENT OF ULTRA-PURE SILICON

THESIS

GEO/PH/78-1

Robert G. Schwein, Jr.
Capt. USAF

Approved for public release; distribution unlimited

78 06 15 072

GEO/PH/78-1

MAGNETORESISTANCE AND HALL
MEASUREMENT OF ULTRA-PURE SILICON

THESIS

Presented to the Faculty of the ~~School of Engineering~~
of the Air Force Institute of Technology
Air University
in Partial Fulfillment of the
Requirements for the Degree of
Master of Science

by

Robert G. Schwein, Jr., B.S.E.E.

Capt.

USAF

Graduate Electro-Optics

December 1977

Approved for public release; distribution unlimited

Acknowledgements

I find a great deal of satisfaction in knowing the many very talented people who have helped in the work that contributed to this thesis. My adviser, Dr. T. Luke, arch-enemy of procrastination, always seemed to have two key phrases, "derive the equation!" and "what were the assumptions?". With that urging how could I not have a better theoretical understanding of what I was to do in the laboratory and for this he has my sincerest thanks. Across the street in the laboratory three new phrases, "measurement-error," "check the equipment," and "collect more data!" became my constant companions while working with Dr. P. Hemenger. A finer friend and tutor cannot be found in the art of engineering, the experimental system, and accurately collecting the data. A tremendous amount of knowledge was gathered by me just from the example he set; for this I find it impossible to thank him enough. The circle is complete with Dr. B. Green who would say "Compare the data with the theory." His guidance during my attempts at understanding the physical meaning of my results provided understanding; I will always be grateful.

Patience and attention to detail are assets of Mrs. O. Davis, typist and linguist, who has taken my chicken-scratched hieroglyphic carvings and transformed them into the clear text, while adhering to the numerous regulations that dictate the format of every page. I find it easy to save the best for last, so when I say that I appreciate the extra time she has given me, I say it with a great deal of meaning.

Robert G. Schwein, Jr.

Contents

	Page
Acknowledgements	ii
Abstract	iv
I. Introduction	1
II. Theory	3
III. Sample and Equipment System Design	18
Sample	18
Equipment System	19
IV. Data Acquisition and Analysis Procedures	21
V. Results	25
Samples	25
Carrier Concentration	25
Hall Coefficient Factor	27
VI. Conclusions	30
Laue Photographs, Hall Bar Shape	30
Magnetic-Field Intensities	30
Magnetoresistance "Master Curve"	31
Bibliography	33
Appendix A: Experimental System and Component List . .	34
Appendix B: Sample Holder Schematic	36
Appendix C: Hall/Van der Pauw Interface Schematics . .	37
Appendix D: Data	48
Vita	63

ACCESSION for	
NTIS	White Section <input checked="" type="checkbox"/>
DDC	Buff Section <input type="checkbox"/>
UNANNOUNCED	<input type="checkbox"/>
J. S. I. CATION	
BY	
DISTRIBUTION/AVAILABILITY CODES	
SPECIAL	
A	

Abstract

Experimental equipment was designed and built to allow automated galvanomagnetic data acquisition on semiconductor samples with resistances up to 10^{12} ohms. Hall and magnetoresistance data was taken on one p-type silicon sample with Boron impurity partially compensated by Phosphorus. Data was taken in a temperature range of 23° Kelvin to 105° Kelvin with magnetic-field strengths up to 20 Kilogauss. Magnetic-field direction was (111) and current in the sample was (110) or equivalent. Results showed that a 40-microvolt noise level in equipment amplifiers obliterated most weak-field data, and possible sample inhomogeneity caused unpredicted strong-field data trends.

The measured total impurity concentration was $2 \times 10^{12} \text{ cm}^{-3}$ and data analyses showed that weak-field measurements must be made with magnetic-field strengths less than 50 gauss for temperatures less than 60° K and strong-field saturation occurs at approximately 2 Kilogauss. The Hall coefficient factor was calculated from the weak- and strong-field data and results approached theoretical values.

TEN TO THE 12TH POWER

deg

I. Introduction

The purpose of this thesis is to establish the use of magnetoresistance measurements over a narrow temperature range, 77 degrees Kelvin to 100 degrees Kelvin, to assess the impurity content in high purity silicon, i.e., $N_A + N_D \leq 10^{13}$ atoms per cubic centimeter. D. Long, et al. (Ref 5) published research on the technique of using magnetoresistance measurements on silicon at liquid nitrogen temperature. They propose a method whereby one deduces the acceptor and donor concentrations in a sample by combining a measurement of the weak-field transverse magnetoresistance at 77° K with a room temperature resistivity or Hall effect measurement. They construct an empirical "master curve" of magnetoresistance versus impurity density by measuring both quantities on eighteen samples of p-type silicon of net impurity content greater than 10^{13} cm^{-3} and varying degrees of compensation. Silicon samples available for this thesis have total impurity concentrations, $N_A + N_D$ of 10^{11} to 10^{13} cm^{-3} . They are p-type with boron as the acceptor impurity and partially compensated with phosphorus donor atoms. This thesis attempts to extend the "master curve" to include our high-purity samples. It is then necessary to determine if the curve will be a sensitive enough tool in this high purity region to use the methods of deduction proposed by D. Long, et al.

Galvanomagnetic data, including Hall Voltage and

Magnetoresistance, is measured on available silicon samples in magnetic fields up to 20 Kilogauss and temperatures up to 120° K. The silicon wafers are factory-cut with the [111] direction perpendicular to the plane of the wafer. Consequently, the magnetic-field direction will be [111] and current directions will be $[1\bar{1}0]$ or equivalent.

At each temperature and magnetic-field strength where a magnetoresistance measurement is to be made an additional measurement, the Hall voltage, is taken to measure the Hall coefficient factor as a function of temperature for each sample. The Hall coefficient factor, which is the ratio of Hall to conductivity mobility, is a quantity of great interest in characterizing the behavior of semiconductors and has yet to be measured in silicon samples of the purity studied in this thesis.

Since galvanomagnetic measurements are to be made on samples with extremely high resistivities, greater than 10^{10} ohm-cm, it is necessary to design and construct special purpose equipment that will convert the sample's high output impedance into a low impedance signal source. This must be done to prevent the volt-meters and current-meters from loading the sample and causing incorrect signal voltages at the input terminals of the measuring equipment.

This thesis is divided into five major parts:

- (1) Theory; (2) Experiment System and Equipment Design;
- (3) Data Acquisition and Analysis Procedures; (4) Results;
- (5) Conclusions.

II. Theory

This section will explain the sequence of measurements and calculations that must be made to extend the "master curve" to include our high-purity silicon. In addition, we define the galvanomagnetic quantities and discuss the sample geometry. The last part of this theoretical section interprets the microscopic phenomenon occurring when charge carriers in the silicon crystal lattice are influenced by electric and magnetic fields.

The Master Curve is an empirical plot of measured weak-field transverse magnetoresistance, M_t vs. measured ionized impurity concentration, $(N_A + N_D)_i$ and is illustrated in Fig. 1.

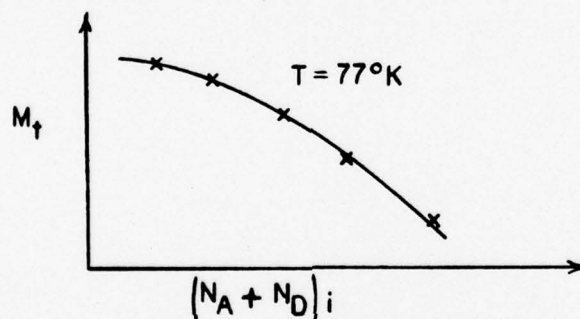


Fig. 1. Master Curve

A single data point in Fig. 1 is the result of the study of a single silicon sample. The quantity $(N_A + N_D)_i$ is calculated from data gathered from a carrier concentration, p vs. inverse temperature, $(T)^{-1}$ plot as represented in Fig. 2.

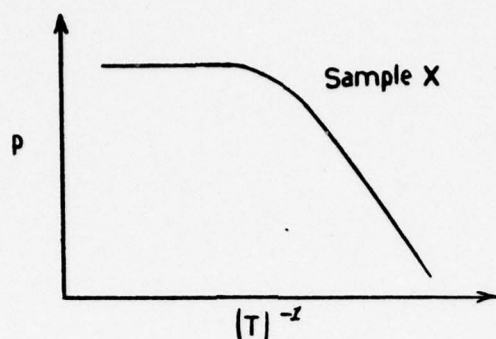


Fig. 2. Carrier Concentration of Sample X

A mathematical model is fitted to the carrier concentration data, the results being values for the sample's acceptor impurity concentration N_A , donor impurity concentration N_D , and acceptor ionization energy E_A . These impurity values and the carrier concentration at 77°K are used to calculate $(N_A + N_D)_i$.

Each carrier concentration data point in Fig. 2 is calculated from the sample's measured Hall data at the corresponding temperature. The Hall data is plotted as shown in Fig. 3.

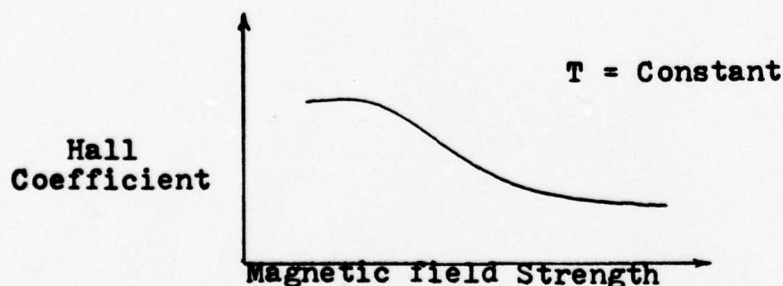


Fig. 3. Constant temperature Hall Coefficient for Sample X

It follows that when there are 30 carrier concentration data points in Fig. 2 then they were calculated from data gathered from 30 constant temperature Hall coefficient

curves similar to Fig. 3.

To illustrate the amount of experimental work necessary to construct the master curve in Fig. 1, we shall briefly discuss the sequence of measurements. Eight voltage measurements are made on the sample for each data point in Fig. 3 and since every plot averaged 30 data points, 240 measurements were taken. The carrier concentration plot, Fig. 2, averaged 20 data points to provide sufficient data for accurate curve fitting calculations. As a result we have made $240 \times 20 = 4800$ measurements on the sample to construct Fig. 2. If only 5 different samples are measured in the construction of the master curve then we have made $5 \times 4800 = 24,000$ measurements. The equipment built to automate the sample data collection is discussed in Appendix C. We now will consider definitions of appropriate galvanomagnetic quantities and their measurement techniques.

Galvanomagnetic measurements are made on silicon samples with the following geometry:

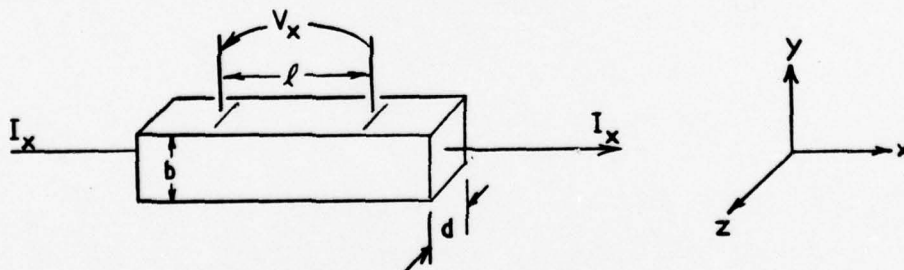


Fig. 4. Sample Geometry

The resistivity is defined as

$$\rho = \frac{V_x}{I_x} \frac{bd}{l} \text{ (ohm-cm)} \quad (3)$$

where V_x is in volts and is measured between two contacts spaced ℓ centimeter apart, I is the current in amperes, and bd is the cross-sectional area in cm^2 . If a magnetic field, B_z , is applied to the sample in Fig. 4 then a Hall voltage, V_H , is generated as shown in Fig. 5.

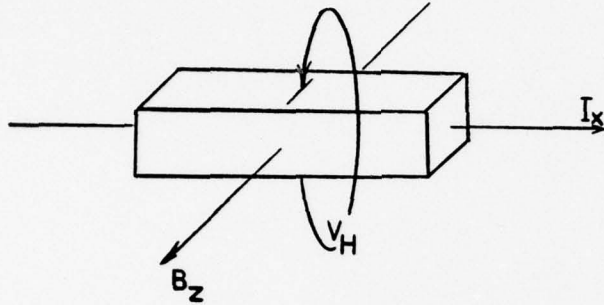


Fig. 5. Hall Voltage Measurement

The Hall coefficient, R , is defined as follows:

$$R = \frac{V_H d}{B I} \left(\frac{\text{cm}^3}{\text{Coulomb}} \right) \quad (4)$$

where V_H is measured in Volts and B in Volt-sec/ cm^2 .

Carrier concentration, p , in units of Holes/ cm^3 is given by the following equation with the assumption that we have a p-type semiconductor and the intrinsic carrier concentration is negligible.

$$p = \frac{1}{Rq} \frac{\langle \tau^2 \rangle}{\langle \tau \rangle^2} = \frac{r}{Rq} \quad (5)$$

Holes, as they move through the crystal lattice, collide with ionized impurities, phonons, and lattice imperfections. τ is the time interval in seconds between scattering events.

The Hall coefficient factor, r , is unitless and indicates the magnitude and an-isotropy of scattering (Ref 7:3324). The electronic charge is q and is equal to 1.6×10^{-19} coulomb.

Hall mobility, μ_H and drift mobility, μ are defined as follows:

$$\mu_H = R\sigma \left(\frac{\text{cm}^2}{\text{Volt-Sec}} \right) \quad (6)$$

$$\mu = \frac{R\sigma}{r} \left(\frac{\text{cm}^2}{\text{Volt-Sec}} \right) \quad (7)$$

$$\sigma = \frac{1}{\rho} \quad (\text{ohm cm})^{-1} \quad (8)$$

The "weak-field" transverse magnetoresistance coefficient, M_t , is defined by the expression:

$$M_t = \frac{\Delta\rho}{\rho_0 B^2} \left(\frac{\text{cm}^4}{\text{Volt}^2\text{-Sec}^2} \right) \quad (9)$$

Resistivity measured at zero magnetic field is designated ρ_0 , and the term $\Delta\rho$ is the increase of the resistivity over the zero-field value, ρ_0 , when a field of magnitude B is applied. Transverse magnetoresistance measurements are made with the current I_x perpendicular to the magnetic flux lines.

The magnetic field B will exert a Lorentzian force on the holes as the holes move in the direction of current I_x . Holes will have a velocity in the y direction v_y as well as the x direction v_x . The expressions for v_x and v_y can be derived directly from the equation of motion for a hole in

the presence of both a steady electric field \bar{E} and a steady magnetic field \bar{B} (Ref 6:282-284). With those results and Eq (4) we may obtain, assuming a single carrier in a spherical band

$$R = \frac{q}{m^*c} \frac{\overline{\tau_p^2 / (1 + \omega_o^2 \tau_p^2)}}{\tau_p / (1 + \omega_o^2 \tau_p^2)} \frac{E_x \text{ bd}}{I_x} \quad (10)$$

where τ_p is the velocity dependent relaxation time of holes and $\omega_o = qB/m^*c$. m^* is the effective mass of holes in silicon. When the assumption is made that $\omega_o \tau_p \ll 1$ then Eq (10) simplifies to

$$R = \frac{q}{m^*c} \frac{\overline{\tau_p^2}}{\tau_p} \frac{E_x}{I_x} \text{ bd.} \quad (11)$$

This is referred to as the "weak-field" Hall coefficient. We can see that the weak-field Hall coefficient is not proportional to the magnetic-field strength B . This is a way to experimentally check that we are still within the area where the weak-field approximations are valid.

Magnetoresistance, when derived using the same techniques as with the Hall coefficient, is proportional to B^2 and B^4 (Ref 6:284). However, by staying within the weak-field approximation, $\omega_o \tau_p \ll 1$, Eq (9) is valid and the magnetoresistance coefficient is proportional to B^2 . For measurements in the laboratory $\omega_o \tau_p$ is equivalent to

$$\omega_b \tau_p = \frac{qB \tau_p}{m^* c} \quad (12)$$

$$= \frac{\mu_o B}{c} \text{ gaussian units} \quad (13)$$

With B measured in gauss and μ_o in $\text{cm}^2/\text{volt-sec}$ μ_o is defined as the drift mobility in the limit as B approaches zero gauss. The weak-field condition is defined as follows:

$$\frac{\mu_o B}{10^8} \ll 1. \quad (14)$$

The Hall coefficient factor r_B from Eq (5) can be determined experimentally by the relation (Ref 1:103)

$$\frac{R_B}{R_{\infty}} = r_B \quad (15)$$

R_B is the Hall coefficient at the magnetic-field intensity of B gauss and R_{∞} is the Hall coefficient as $B \rightarrow \infty$.

Previous research on R_{∞} and r_B has been compiled and edited (Ref 1:189-212) for Silicon and Germanium samples with impurity concentrations of 10^{13} to 10^{14} (impurities/ cm^3). Since these impurity concentrations are several orders of magnitude greater than the ones measured here, we have been able to measure R_{∞} up to temperatures of 60°K with magnetic fields of 6 kilogauss. The r_B from Eq (15) is significant because we may use it to calculate the carrier concentration p (Holes/ cm^3) in Eq (5), instead of using assumed values (Refs 5:355; 8:97) of r_B . A symbol r_o

will be used to express the value of r_B in the limit as B approaches zero.

As a brief review, the needed Hall and magnetoresistance relations are listed below:

$$\text{conductivity } \sigma = \frac{1}{\rho} = \frac{I_x \ell}{V_x bd} \quad (3)$$

$$\text{Hall coefficient } R = \frac{V_H d}{BI} \quad (4)$$

$$\text{Hall coefficient factor } r_B = \frac{R_B}{R_{\infty}} \quad (15)$$

$$\text{hole-carrier concentration } p = \frac{r_0}{Rq} \quad (5)$$

$$\text{drift mobility } \mu = \frac{R}{r} \quad (7)$$

transverse magneto-resistance coefficient

$$M_t = \frac{\Delta \rho}{\rho_0 B^2} \quad (9)$$

Silicon that has a dominant impurity of Boron, compensated to some degree by Phosphorus, is a p-type semiconductor. Assuming single, discrete acceptor- and donor-energy levels near the valence and conduction bands respectively, the valence-band hole density, p , versus temperature, T , equation is given as follows (Ref 5:354):

$$\frac{p(p+N_D)}{(N_A-N_D)-p} = \frac{U_v}{4} \exp \left[\frac{-\epsilon_A}{KT} \right] \quad (16)$$

This equation is derived directly from charge neutrality and the assumptions made in the derivation are as follows:

1. The number of unionized donor sites equals zero.
2. The Boltzmann approximation is valid meaning $(\epsilon_f - \epsilon_v) \gg KT$.
3. The intrinsic carrier concentration equals zero.
4. The valence-band energy level ϵ_v is referenced at zero electron volts.

N_A and N_D are concentrations of acceptor- and donor-impurities in cm^{-3} , ϵ_A is the acceptor ionization energy in electron volts, and U_v is the effective density of states in the valence band given by the relation (Ref 6:266):

$$U_v = 2 \left[\frac{2\pi m_d^* KT}{h^2} \right]^{3/2} \quad (17)$$

m_d^* is the density-of-states effective mass of holes, K is Boltzmann's constant, and h is Planck's constant. The intrinsic-carrier concentration was assumed to be equal to zero when Eq (16) was derived. Experimental data in this thesis show this assumption is valid when T is less than 120° Kelvin for total impurity concentrations ($N_A + N_D$) of 10^{12} atoms/ cm^3 and less.

A typical graphical depiction of Eq (16) is shown in Fig. 6.

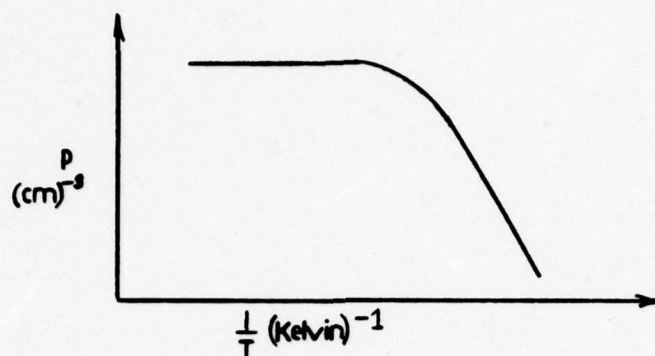


Fig. 6. Typical Plot of Equation 16

Laboratory measurements of the carrier-concentration p when plotted as a function of temperature will match Fig. 6. Values of N_A , N_D , and ϵ_A are found by least-squares curve-fitting techniques that will cause the theoretical model, Eq (16), to reproduce the laboratory data. In this manner we may derive the acceptor N_A and donor N_D impurity concentrations for each studied sample.

The straight-slope low temperature portion of Fig. 6 is where $p \ll N_D$. At this low temperature we are in the "freeze-out" region of the semiconductor's galvanomagnetic characteristics (Fig. 7), and Eq (16) reduces to the following linear equation in p .

$$p = \frac{(N_A - N_D)}{N_D} \frac{U_V}{4} \exp \left[\frac{-\epsilon_A}{KT} \right] \quad (18)$$

The "extrinsic" region of the semiconductor is defined at the temperatures where the total impurity concentration $N_A + N_D$ is fully ionized, but the intrinsic carrier-concentration is negligible.

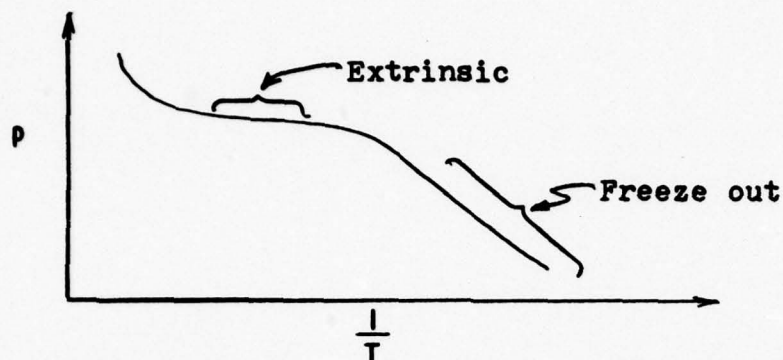


Fig. 7. Extrinsic and Freeze-out Characteristics

The slope of the extrinsic region is equal to zero and the extrinsic carrier concentration is equal to $N_A - N_D$.

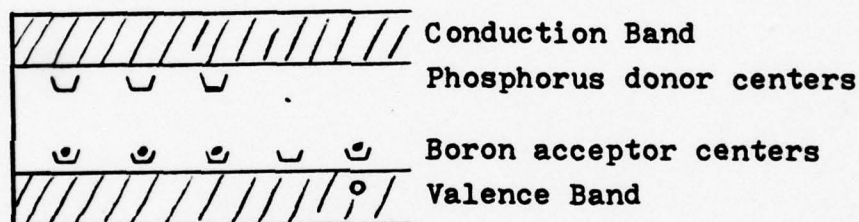


Fig. 8. Model of Single, Discrete Acceptor and Donor Energy Levels Near the Valence and Conduction Bands

In the example of Fig. 8 the concentration of donor impurities N_D equals 3 phosphorus atoms and acceptor impurities N_A equals 5 Boron atoms. The total impurity concentration in this silicon example is $N_A + N_D$ or 8 atoms. At temperatures of absolute zero and above the donor levels will be completely ionized, therefore the minimum ionized-impurity concentration $(N_A + N_D)_i$ is equal to $2N_D$. As the sample temperature increases there will be enough energy to excite electrons from the valence band to the acceptor

levels; as a result, p number of holes are generated in the valence band and a p number of acceptor centers have been added to the ionized-impurity concentration.

$$(N_A + N_D)_i = 2N_D + p \quad (19)$$

The primary scattering mechanisms in the silicon samples used in this thesis are assumed to be lattice scattering and impurity scattering. Oxygen and other impurities other than boron and phosphorus were present in quantities so small as to be immeasurable. Oxygen occupying interstitial lattice sites may have been present in appreciable concentrations without being detected. Silicon-lattice imperfections were measured by etching techniques and shown to be less than 1000 per square centimeter. These measurements were made on samples cut from the same boole as the samples used in this thesis.

Holes that move under the influence of a steady electric field, for illustrative purposes, can be pictured as moving in a linear motion from the point where they were injected into the sample to the point where they are collected and the charge rate of flow is measured in a current meter. Since the holes are moving directly from point A to point B they will be scattered by the impurities and lattice that lies along their linear path.

When a magnetic field is applied to the sample then the holes will move through the lattice under the influence of the forces parallel to the electric field and parallel

to the vector cross-product of the electric and magnetic fields. The curvilinear hole-motion in effect increases the path length between the point of injection and the point of measurement and thus increases the number of scattering events. Under the influence of a constant electric field the increase in hole-scattering is perceived as a decrease in the charge rate of flow. When compared with measurements made with zero magnetic field the sample resistance to current flow will have appeared to increase and this increase in resistance is defined as magnetoresistance. When two samples with different impurity concentrations are placed in identical conditions of temperature and magnetic fields the measured magnetoresistance between the two samples will be different, the difference depending on the phosphorous and boron concentrations.

The magnetoresistance coefficient given by Eq (9)

$$M_t = \frac{\Delta \rho}{\rho_0 B^2} \quad (9)$$

is a ratio of the increased resistivity $\Delta \rho$ in the magnetic field B to the zero magnetic field resistivity ρ_0 .

Because of this, the magnetoresistance cannot be equated to the total impurity concentration ($N_A + N_D$) in the sample.

An infinite number of combinations of N_A and N_D can yield the same sum of total impurity concentration ($N_A + N_D$), yet the magnetoresistance of each sample under otherwise identical conditions will be different.

The degree of acceptor-impurity compensation by the donor impurity as well as the number of carriers available for scattering are the differences between samples that would have the same total impurity concentrations, but different magnetoresistance coefficients.

Thus a quantity that would be unique among samples that had identical $N_A + N_D$ would be $(N_A - N_D) - p$ which is the number of uncompensated acceptors minus the carrier concentration. Aside from completely characterizing a sample's scattering characteristics for a given $N_A + N_D$ under the limited scope examined in this thesis, the quantity turns out to be in fact the unionized (neutral) impurity concentration. Accordingly, to uniquely characterize samples over a wide range of total impurity concentrations Eq (20) is used:

$$(N_A + N_D)_i = (N_A + N_D) - [(N_A - N_D) - p] \quad (20)$$

which is the ionized impurity concentration, also given in Eq (19) in different form.

As a result we can expect to derive a unique empirical relation between the measured magnetoresistance and the ionized impurity concentration over a wide range of impurity concentrations (Fig. 9).

The quantities $(N_A + N_D)$ and $(N_A - N_D)$ are characteristic of a given sample and are not temperature-dependent. Carrier-concentration p is a function of temperature, therefore $(N_A + N_D)_i$, Eq (20), is also temperature-dependent.

Boiling liquid nitrogen, 77°K , was used by D. Long (Ref 5) as a convenient temperature to use when measuring the magnetoresistance and carrier concentration of the 18 silicon samples he studied. His samples allowed him to construct Fig. 9 for $(N_A + N_D)_i$ greater than 10^{13} cm^{-3} , whereas this thesis extends his curve into the region where $10^{10} < (N_A + N_D)_i < 10^{13}\text{ cm}^{-3}$.

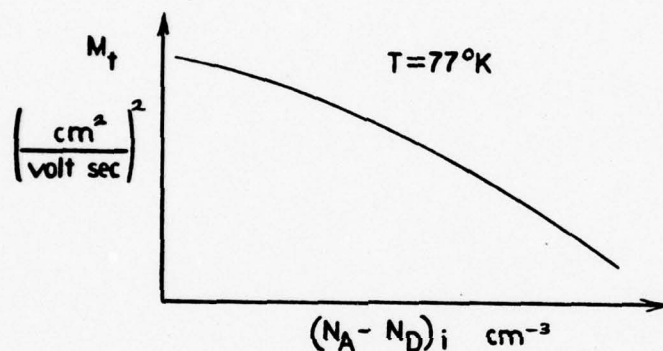


Fig. 9. Example of the "Master Curve." Weak Field Magnetoresistance Coefficient vs. Ionized Impurity Concentration at Liquid Nitrogen Temperature

III. Sample and Equipment System Design

Sample

The silicon sample was cut with an ultrasonic cutter into the form shown in Fig. 10(A) (dimensions in mm.).

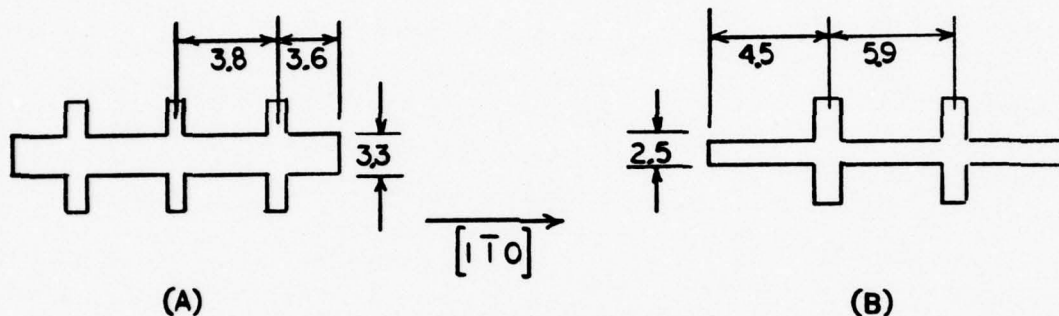


Fig. 10. Silicon Bridge Designs

When the laser-cutting facilities became unexpectedly available from North American Rockwell, California, the sample shape in Fig. 10(B) was designed by us and sent to be cut. The advantages of the latter design are twofold, first, the length takes maximum advantage of our insulated sample holder area, and second, the measurement arms are far removed from the transverse currents caused by electrode shorting at the two ends. Data used in the design was taken from A. C. Beer (Ref 1:57). Magnetoresistance measurement error of 2% was calculated for Design (A) and 0.1% for Design (B). All samples were orientated with Laue diffraction patterns taken by us with the x-ray facilities in the Materials Laboratory. Data used to interpret the Laue diffraction patterns came from E. A. Wood (Ref 10:56)

and maximum estimated orientation error after sample cutting was ± 1 degree. The procedures used to contact the gold signal probes to the silicon sample were developed by the personnel in the Materials Laboratory. These procedures are given in detail in Reference 2.

Equipment System

Equipment and system designs used to measure and control the experiments are listed and illustrated in Appendix A. The sample with sample holder are contained in a Janis dewer. Vapor from boiling liquid helium passes over the sample; heaters in close proximity control the sample temperature. Care was taken to ensure isothermal sample temperatures and details on the sample-holder design are given in Appendix B.

Resistances over 10^{12} ohms are encountered in the silicon samples studied in this thesis. As a result, extraordinary measures have to be taken to make galvanomagnetic measurements but avoid sample loading by the measuring equipment. The guarded approach involves the use of a high input impedance unity gain amplifier between each probe on the sample and the external circuitry, thus permitting measurement with standard laboratory differential voltmeters. Further, the unity gain outputs drive the shields on the leads between the amplifier and sample which reduces leakage currents and dramatically reduces the system's time constant by effectively eliminating stray capacitance in the leads (Ref 3:698).

A guarded Hall system requiring three unity gain amplifiers is shown schematically in Fig. 11.

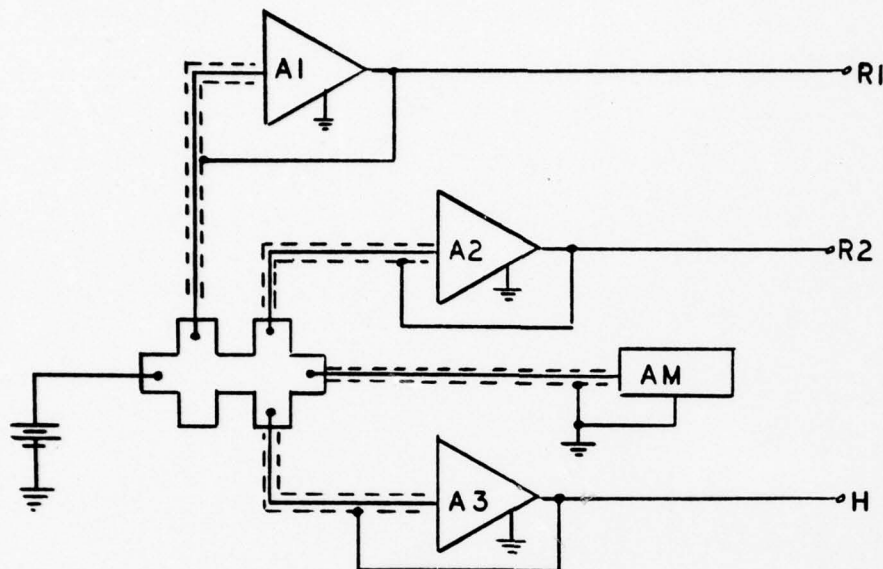


Fig. 11. Guarded Hall System Employing Three Unity Gain Amplifiers A1, A2, and A3

The current is measured by an electrometer ammeter, AM, operated in a feedback mode which drives the input to ground, thus negating the need for guarding the current lead. The voltage for calculating the resistivity is measured between R1 and R2, while the Hall voltage is measured between R2 and H with the magnetic field on. A circuit of this type permits routine measurement of high resistivity samples (Ref 3:698). This circuit is the basis for the interfacing system design developed for this thesis that includes current reversing features, van der Pauw configuration compatibility, and computer control options. This interfacing system is detailed in Appendix C.

IV. Data Acquisition and Analysis Procedures

Keithley Electrometer unity gain amplifiers are adjusted for a gain of one by connecting their input to the low terminal of a differential voltmeter and their output to the high terminal. The gain is adjusted until the voltmeter reads zero.

Hall bar wire contacts are checked by looking at their electrical characteristics at several temperatures over the intended range of operation. Several problems can occur. A bad contact at low temperatures can become electrically insulated from the silicon sample. A voltmeter measuring a signal on this line will suddenly begin varying randomly with noise at the moment the contact becomes an insulator. This problem, when present, usually disappeared above 100 degrees Kelvin. A second problem encountered is a rectifying contact (s). With current flowing in one direction, a measured voltage between two sample probes will be small but with the current reversed, the voltage can be twice as large, and up to several orders of magnitude larger in a severe case.

After it is determined that the sample contacts are ohmic over the range of temperatures, the sample will be studied. Adjust the helium rate of flow to minimum required to reach the lowest desired temperature. With the sample heaters off, the helium valve on the dewer is opened just enough to stabilize the sample temperature at a point

just below the lowest temperature expected. We chose a temperature of about 15° Kelvin. The heaters are used to warm the sample to the lowest temperature desired and the heater controller will adjust heater power for helium vapor flow fluctuations.

Magnetoresistance as well as conventional Hall measurements are taken at every 3 degrees, beginning at 20° Kelvin up into the samples extrinsic region of 110° Kelvin. In the temperature range of 20° K to 30° K magnetoresistance measurements are taken at 50 gauss increments and at temperatures above 30° K measurements are taken at 100 gauss increments. Because we record magnetoresistance data at low temperatures in incremental magnetic fields, Hall voltage is also recorded at these magnetic fields. This provides a side benefit of determining the Hall coefficient factor.

The sample temperature is kept constant at a desired value by a temperature controller (Appendix A). Germanium and platinum thermometers are used by the controller to sense the sample temperature. The germanium thermometer is sensitive to magnetic fields and when this field is turned on the controller will sense a false temperature drift. After taking a galvanomagnetic measurement with the magnetic field on it is necessary to turn the field off and check the sample temperature. The controller does not cause more than $1/8$ degree K drift in sample temperature while the magnetic field has been set at 20 Kilogauss for 3 minutes.

We have written extensive data checking and reduction computer programs to provide quick analysis so that we may repeat measurements if this appears warranted. The Hall coefficient, and magnetoresistance as a function of magnetic field strength is plotted for every temperature studied. In addition, the resistivity, Hall mobility, weak-field Hall coefficient, weak-field Hall coefficient factor, weak-field magnetoresistance coefficient, and hole density as a function of temperature are plotted. This analysis, approximately 30 graphs, is available within hours after finishing the sample study for a given temperature. On several occasions this has pointed to contact problems, temperature instabilities at higher magnetic field strengths, as well as reverse sample current not being exactly equal to forward current at some data points. The latter problem proves especially troublesome at temperatures less than 30° K at magnetic fields greater than 5 Kilogauss. A change of one nanoampere in current magnitude produced a several millivolt change in Hall and resistivity voltages.

After collecting data that cover the extrinsic and freeze-out regions in the sample, we make an additional check on the validity of the results. Eq (16) is fitted with least-squares techniques to the hole concentration data calculated with Eq (5). Comparison of ϵ_A with the accepted value for Boron provides an excellent check on the data validity.

By studying a number of samples of varying impurity

content and degree of compensation we can construct the empirical curve of magnetoresistance vs. ionized impurity concentration at liquid nitrogen temperature, 77° K.

V. Results

Samples

Galvanomagnetic measurements were attempted on three samples before this thesis deadline. Two samples had contacts that became insulators below 60° K. As a result, necessary data could not be gathered from the freeze-out region, less than 40° K, and the extrinsic region 50° K to 100° K, which is necessary in order to derive the boron activation energy and the $N_A - N_D$ value. The third sample, C, from which the data in this thesis was taken, had contacts that remained ohmic down to 23° K. A discussion and graphical depiction of pertinent data is presented in Appendix D. One day was consumed for each temperature that data was taken, results being available the next morning for analysis and to provide direction for further study that day.

The hot-carrier phenomenon was avoided by ensuring that applied voltage across the sample bridge was in the region where an incremental change would produce a linear incremental change in current. The maximum electric field allowable in the sample was determined for each temperature, the results averaged 1 volt-cm.

Carrier Concentration

From the plot of carrier density versus temperature (Fig. 12) we see that liquid nitrogen temperature, 77° K, lies within the extrinsic region of the curve. The

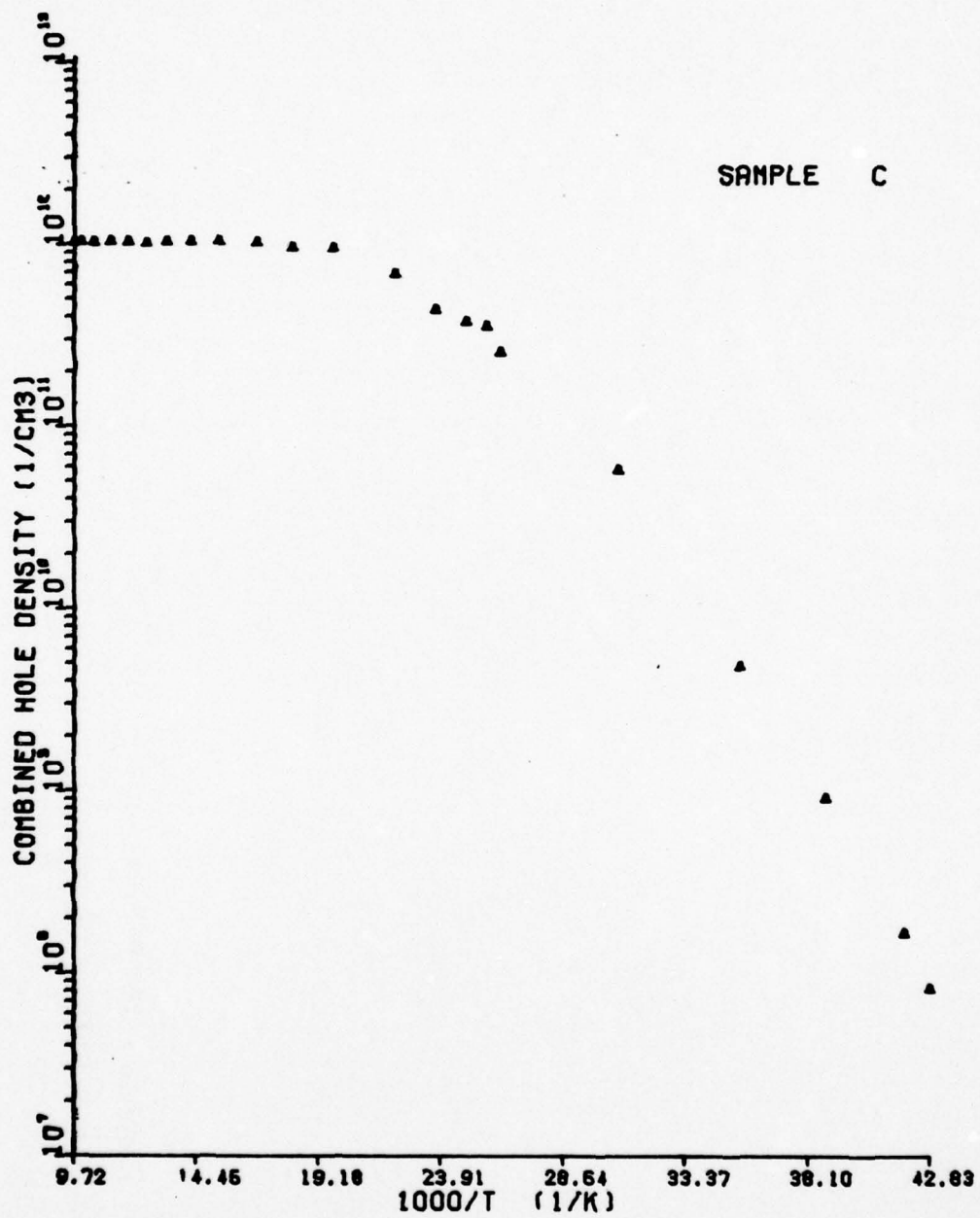


Fig. 12. Carrier Concentration

procedure outlined by D. Long, et al. (Ref 5) depended on the liquid nitrogen temperature being in the silicon's freeze-out portion of the carrier concentration plot. It is probable that ambiguity will exist when calculating our sample's total impurity concentration, $N_A + N_D$, from a measured magnetoresistance value at 77° K. A simple thought-exercise might illustrate this point. Given two silicon samples, A and B, where 77° K was within their extrinsic regions and both samples had the same total impurity concentrations, $N_A + N_D = 7$, suppose that sample A had $N_D = 1$, $N_A = 6$ and sample B had $N_D = 3$, $N_A = 4$. In the extrinsic region at 77° K sample A would have 5 holes and sample B would have 1 hole as majority carriers. We should have very different values of magnetoresistance between the two samples, yet both samples have the same $N_A + N_D$. As a result any attempt to construct a master curve that plotted magnetoresistance versus ionized carrier concentration $(N_A + N_D)_i$ would lead to ambiguous results. In the extrinsic region $(N_A + N_D)_i = N_A + N_D$. We could have multiple values of magnetoresistance for identical values of $N_A + N_D$. Certainly additional data from different samples can be used to support or refute this hypothesis.

Hall Coefficient Factor

A benefit of measuring the Hall coefficient at magnetic field strengths where the difference in mobility between the heavy and light hole band is negligible is that the Hall coefficient now involves only the sum of the carrier

densities. This provided us with data to calculate the Hall coefficient factor by the use of Eq (15).

$$r_0 = \frac{R_0}{R_{\infty}} \quad (15)$$

Results of these calculations are plotted in Fig. 13. Below 33° K it became increasingly difficult to estimate the weak-field Hall coefficient R_0 due to the noise problems discussed in greater detail in Appendix D. Simple algebraic manipulation of Eq (15) will show that r_0 is the ratio of drift mobility to Hall mobility; therefore it should not increase as temperature decreases. Of particular interest is that the data above 33° K is within 5% of the theoretical values calculated by the personnel at the Air Force Materials Laboratory and by A. C. Beer (Ref 1: 164-174, 195-212). Current research with a variety of silicon samples of varying impurity concentrations will refine this existing data and extend it over a wider temperature range.

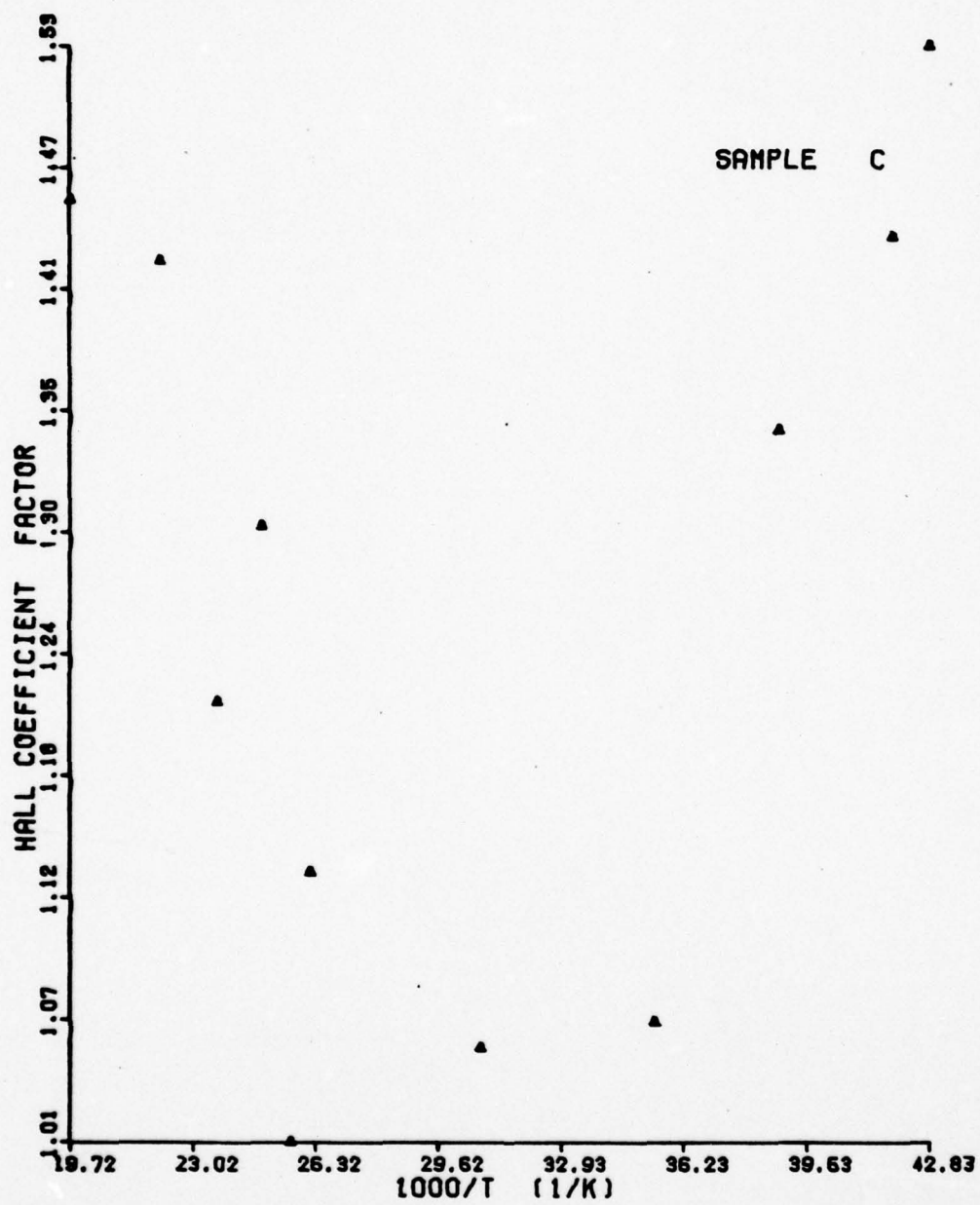


Fig. 13. $\frac{R_0}{R_\infty}$

VI. Conclusions

Based on the problems encountered in setting up the experimental equipment and the data gathered on the one sample, a great deal has been learned that can make future experimental magnetoresistance measurements on the high-purity silicon much smoother and more productive.

Laue Photographs, Hall Bar Shape

With the current facilities Back-Reflection Laue Photographs take two hours to expose, but a change of x-ray tubes could reduce the time to two minutes. The shape of the Hall bar bridge cut with the currently available ultrasonic cutting dies does not take maximum advantage of the Beryllium oxide wafer area. Considering that very weak magnetic-field strengths will be necessary to measure the weak-field Hall and magnetoresistance coefficients and that signal levels are on the order of microvolts, a sample bridge shape that optimizes the length to width ratio would be very desirable.

Magnetic-Field Intensities

Magnetic-field strengths of 10 to 20 Kilogauss require extra precautions not normally considered when working with a magnet that has a maximum field strength of 6 Kilogauss. It would probably be wise to electrically insulate with teflon tape any exposed copper in the sample holder that is near the uninsulated sample probes. This, in addition to

keeping the uninsulated signal-probe wires very short, should prevent these wires from electrically shorting against the copper sample holder when the wires flex under the influence of high-magnetic fields.

The coto-coil relays used in the interfacing system will close in the presence of an external magnetic field of 15 gauss when the flux lines are parallel to the direction of the reeds. When working with a 20-Kilogauss magnet, the physical placement of any equipment with relays must be planned carefully.

The sample heaters are embedded in the sample holder directly in the path of the magnetic flux-lines as the lines cut in a perpendicular direction through the sample (Appendix B). Since we have now concerned ourselves with the galvanomagnetic effects at weak magnetic-field strengths, it is possible that the heaters might significantly distort the magnetic field around the sample. After checking the heater composition and its characteristics in a magnetic field, it might be found necessary to move the heaters to points outside the line of flow of the flux lines.

Magnetoresistance "Master Curve"

The method used by D. Long, et al. (Ref 5) to determine the impurity content of silicon will work on the purer silicon if the method is modified, but it will not be a convenient technique to use. A master curve of magnetoresistance versus ionized impurity concentration should be developed at a temperature well within the freeze-out region;

25° K is a good possibility because at 33° K the hole-density curve begins to level off into the extrinsic region. The room-temperature resistivity measurement to obtain $N_A - N_D$ as suggested by D. Long will not work for our samples. At 125° K the pure silicon in our study begins to move rapidly into the intrinsic conduction region, a situation not encountered by the earlier study on samples of less purity. If this magnetoresistance technique is to be studied in greater detail, we recommend that magnetoresistance data be collected within the semiconductor's freeze-out temperature range in addition to that which would normally be collected at 77° K. This additional data would be used in the likely event that the "master curve" is ambiguous when constructed for 77° K.

Bibliography

1. Beer, A. C. Galvanomagnetic Effects in Semiconductors. New York: Academic Press Inc., 1963.
2. Dobbs, B. C., et al. "Ohmic Contacts on High Purity P-Type Silicon." Accepted for publication by Journal of Electronic Materials. Publication date has not been set. Published by Electrochemical Society.
3. Hemenger, P. M. "Measurement of High-Resistivity Semiconductors Using the Van der Pauw Method." Review of Scientific Instrumentation, 44-No6: 689-700 (June 1973).
4. Lee, P. A. "Determination of the Impurity Concentrations in a Semiconductor from Hall Coefficient Measurements." British Journal of Applied Physics, 8:340-343 (August 1957).
5. Long, D., et al. "Impurity Compensation and Magnetoresistance in P-Type Silicon." Physics Review, 30-No3:353-362 (March 1959).
6. McKelvey, J. P. Solid State and Semiconductor Physics. New York: Harper and Row, 1966.
7. Ottaviani, G., et al. "Hole Drift Velocity in Silicon." Physical Review B, 12-8:3318-3329 (October 1975).
8. Putley, E. H. The Hall Effect and Semiconductor Physics. New York: Dover Publications Inc., 1968.
9. Sokolov, Y. F. and B. G. Stepanov. "Physical Basis for Using the Magnetoresistance Effect to Measure the Mobility and Concentration of Current Carriers." Mikroelektronika, 4:414-421 (September 1975).
10. Wood, E. A. Crystal Orientation Manual. New York: Columbia University Press, 1963.

Appendix A

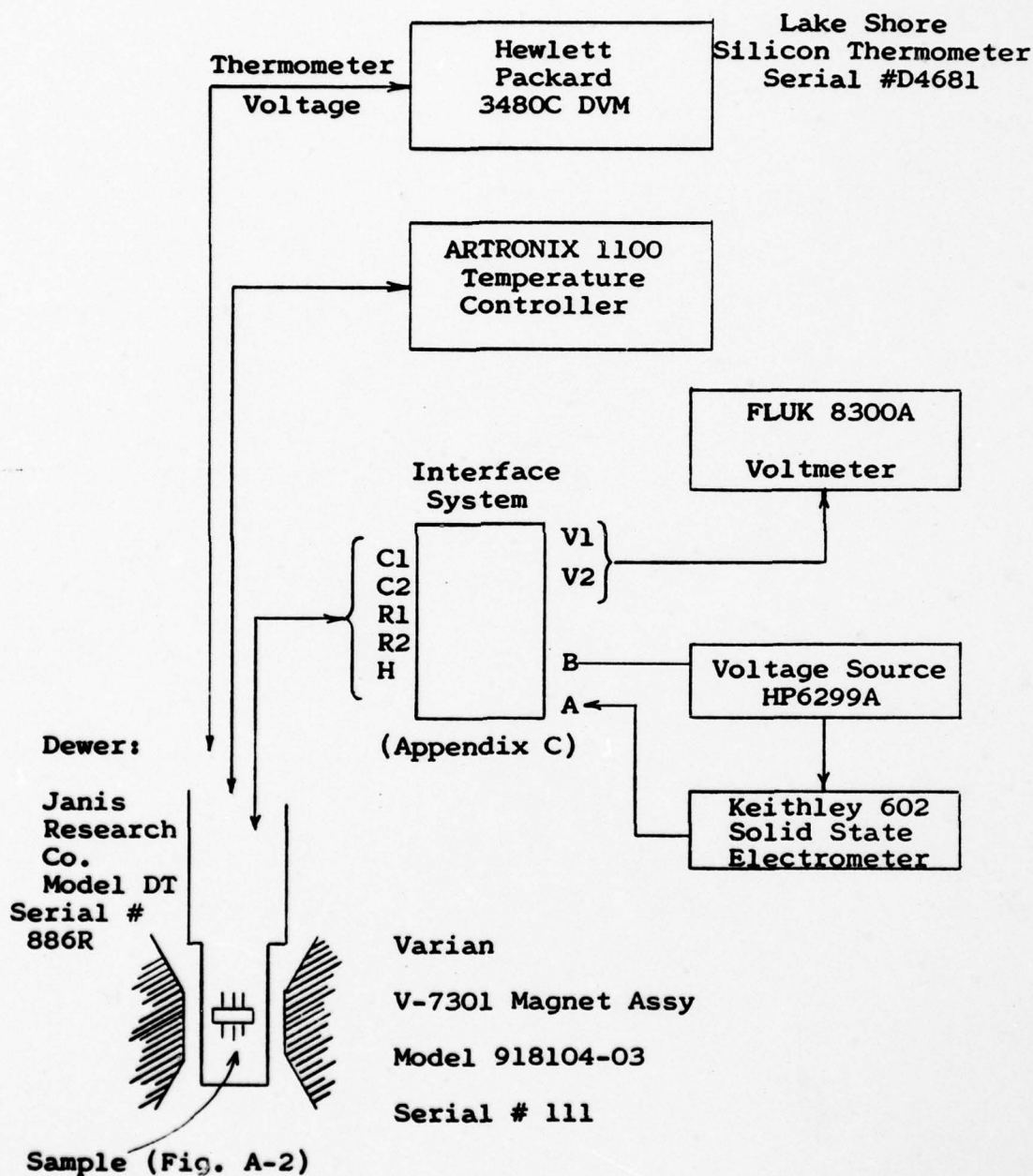
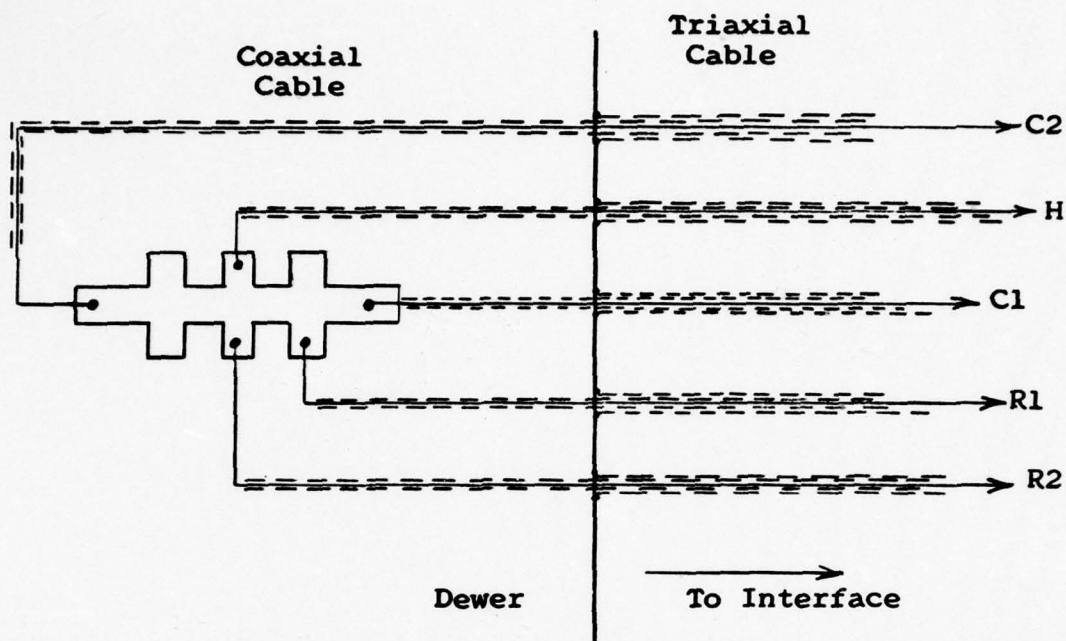


Fig. A-1. Experimental System Design



The Deutsch Company model DM5606-3719P receptacle and DS07-37195-059 Plug.

Fig. A-2. Hall Bar wiring detail

This figure illustrates some of the techniques used to prevent signal leakage to ground. The innershield of the triaxial cable and the outer shield of the coaxial cable are electrically continuous. These shields are driven by the unity gain amplifiers and are at the same potential as their respective inner conductors.

Appendix B

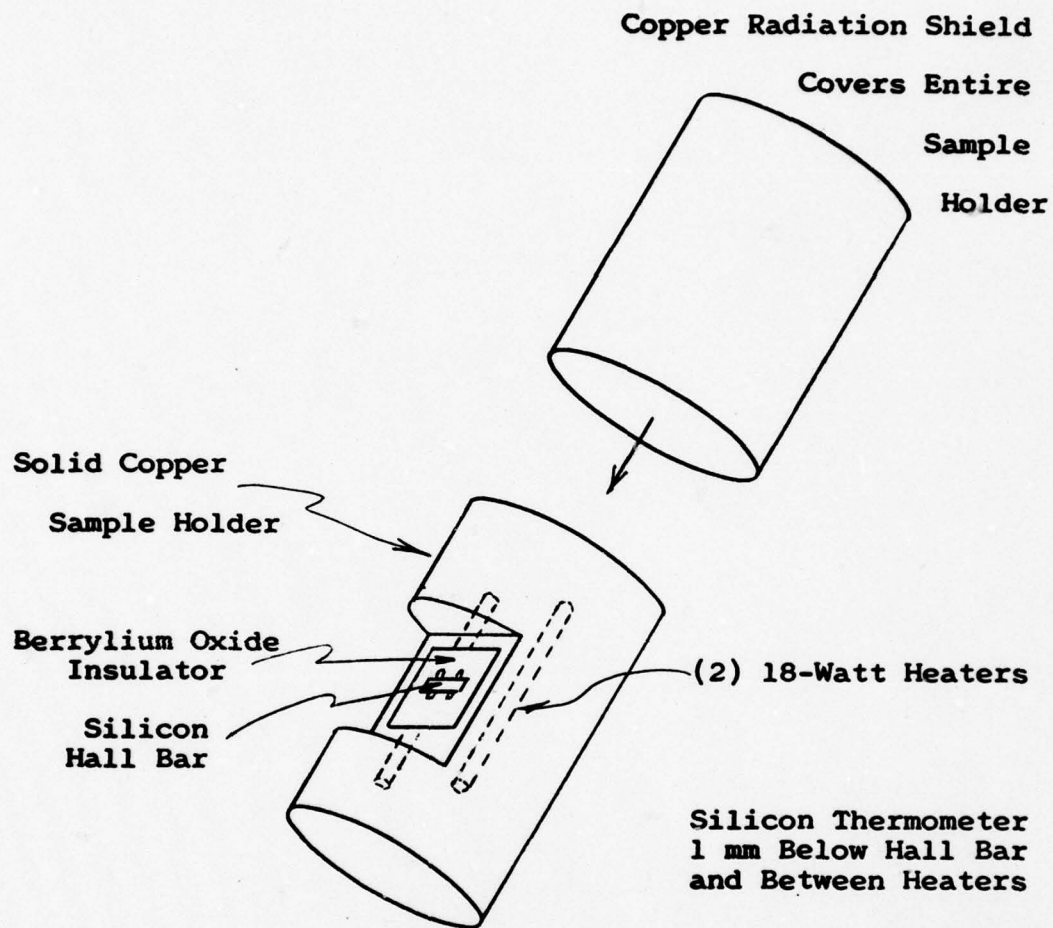


Fig. B-1. Electrical Insulation and Thermal Details of Sample Holder and Radiation Shield

Appendix C

Interface

The Hall/van der Pauw interface system are circuits that isolate a test sample under study from the loading effects of the measuring equipment. This system was designed for, but not limited to, two sample configurations, the van der Pauw cloverleaf, and the Hall bar bridge, Fig. C-1.

The five input ports, R1, R2, C1, C2, and H, are triaxial jacks that accept the triaxial signal and power leads connected to the sample. The four output ports, V1, V2, A, and B, are coaxial jacks two, V1, V2, for the differential voltmeter, one, A, for the current meter and one, B, for the voltage source (power supply). Two modes of operation were designed into the interface system, manual control by a front panel rotary switch or computer control.

Signal Circuits

There are two sample to measuring equipment and power supply interconnection configurations that must be accounted for when making Hall and magnetoresistance measurements on a Hall bar bridge. Additionally, there are six interconnection configurations when working with the van der Pauw cloverleaf (Fig. C-2). An auxiliary requirement is a current reversal feature on all configurations for signal averaging. The connection of the interface's input terminals to the appropriate output terminals for the

desired measurement configuration is made by an 18 relay signal routing circuit (Fig. C-3).

Sample isolation from measurement equipment loading effects is accomplished with two techniques. First, guarding the signal lines from the sample to the interface with the use of triaxial cables that have the inner shield driven to the same voltage as the center conductor (Ref 3) eliminates signal current leakage to ground. The unity gain amplifiers are impedance converters that provide the voltage to the inner shield as well as to the measuring equipment. Secondly, meticulous engineering is used on the interface's signal input circuits. The measured resistance between each center pin of the input jacks and the guard circuits as well as ground is greater than 10^{14} ohms. All triaxial jacks contain Teflon as an insulating medium and all internal signal wires do not touch any other material except air before they reach the input terminals of their unity gain amplifiers. The circuits were constructed on a Clean Bench using standard clean room procedures. Relays were custom designed to the required low leakage and guard specifications and are listed in Fig. C-3.

Control Circuits and Logic

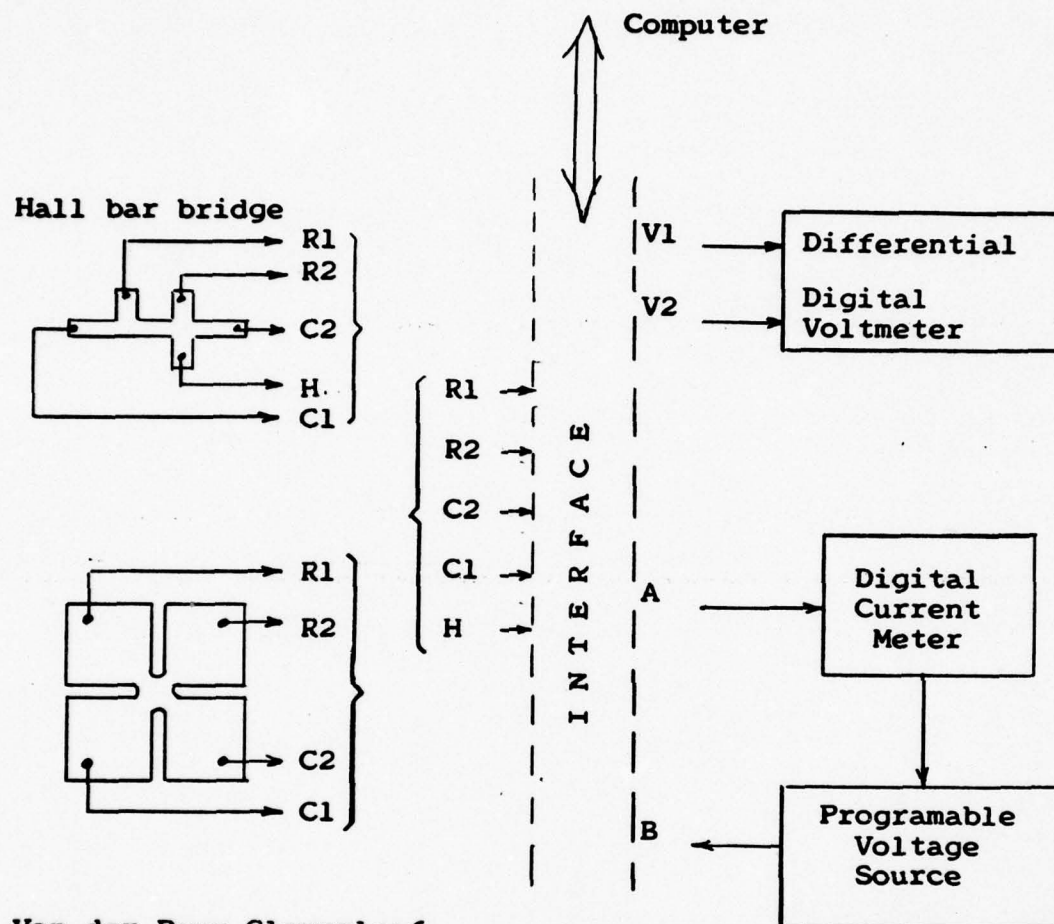
TTL integrated circuit logic is used to control relay actuation either by computer or manual control. The system block schematic is shown in Fig. C-4. IEEE 488 interface standards for programmable data transmitters are used; multi-leaving for half-duplex communication permits a

programmable I/O function. The circuit generates an acknowledge signal that can be used to interrupt the computer.

A ten-position rotary switch on the interface's operator control panel permits the user to select one of the 8 internally programmed relay combinations, corresponding to the 8 sample configurations in Fig. C-2, or to put the interface under computer control. Position ten turns the interface off. A toggle switch, also on the front panel, is used to reverse the current in the sample configuration selected by the rotary switch. This is inoperative when the interface is under computer control as the computer instructions sent to the interface will perform the current reversal operation.

Circuits designed to communicate with the computer and decode the computer commands are illustrated in Fig. C-5 and C-6. The preprogrammed logic for the 8 sample configurations, the switching logic, and the current reversing logic are diagrammed in Fig. C-8. Fig. C-7 shows the logic that accepts computer control or manual control to drive the selected relay coils.

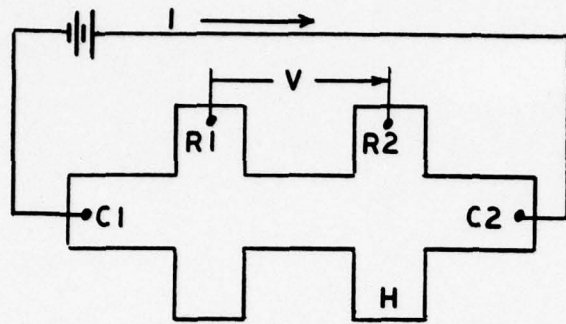
Appendix C



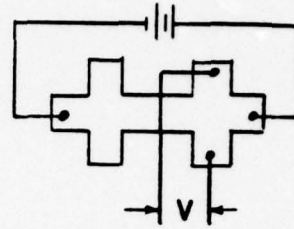
Van der Pauw Cloverleaf

Fig. C-1. Hall/Van der Pauw Interface

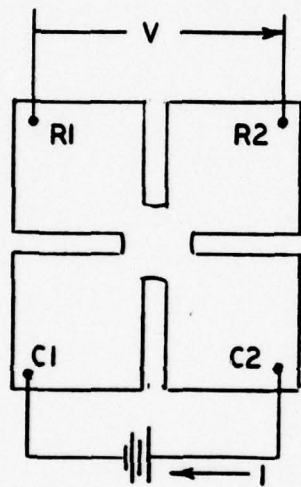
This illustration shows the purpose of the nine signal ports of the interface and their respective coded designations. The computer is used in the automated experimental system.



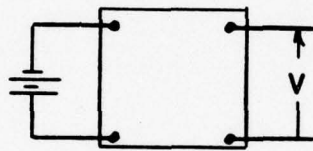
(1)



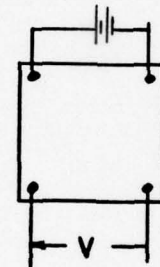
(2)



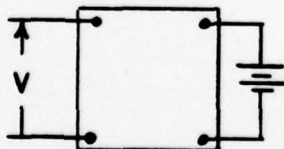
(3)



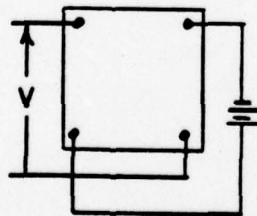
(4)



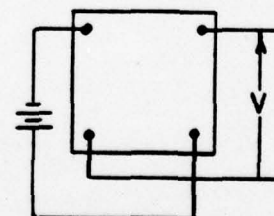
(5)



(6)



(7)



(8)

Fig. C-2. Two Hall Bar Configurations and Six Van der Pauw Cloverleaf Configurations Selected by Operator Control

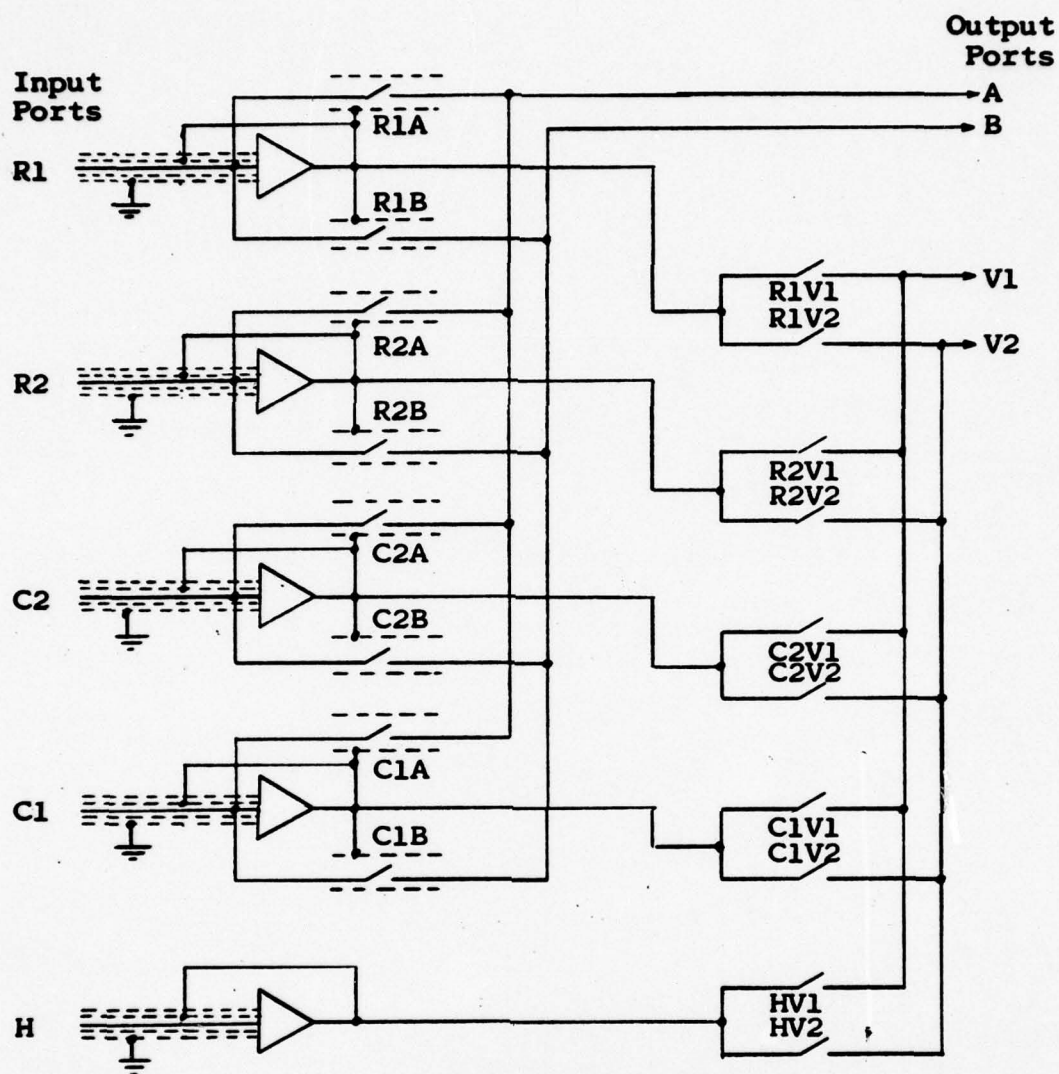


Fig. C-3. Hall/van der Pauw Interface Signal Paths

Relays: Coto-Coil, model U-12-4 relay with coaxial shield.

Unity gain amplifiers: Keithley, model 610C Solid-State Electrometer.

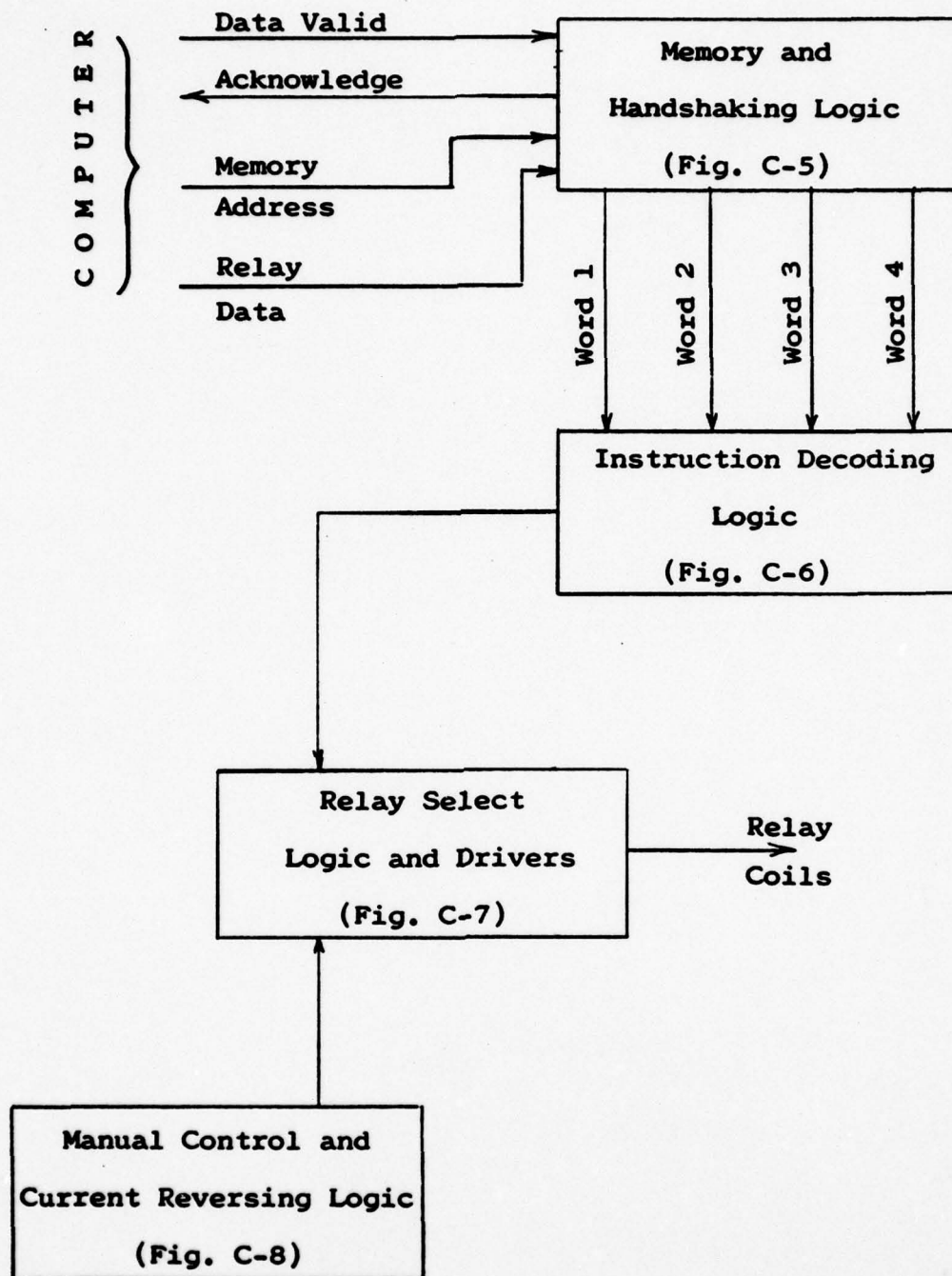


Fig. C-4. Interface System Electronics--Block Diagram

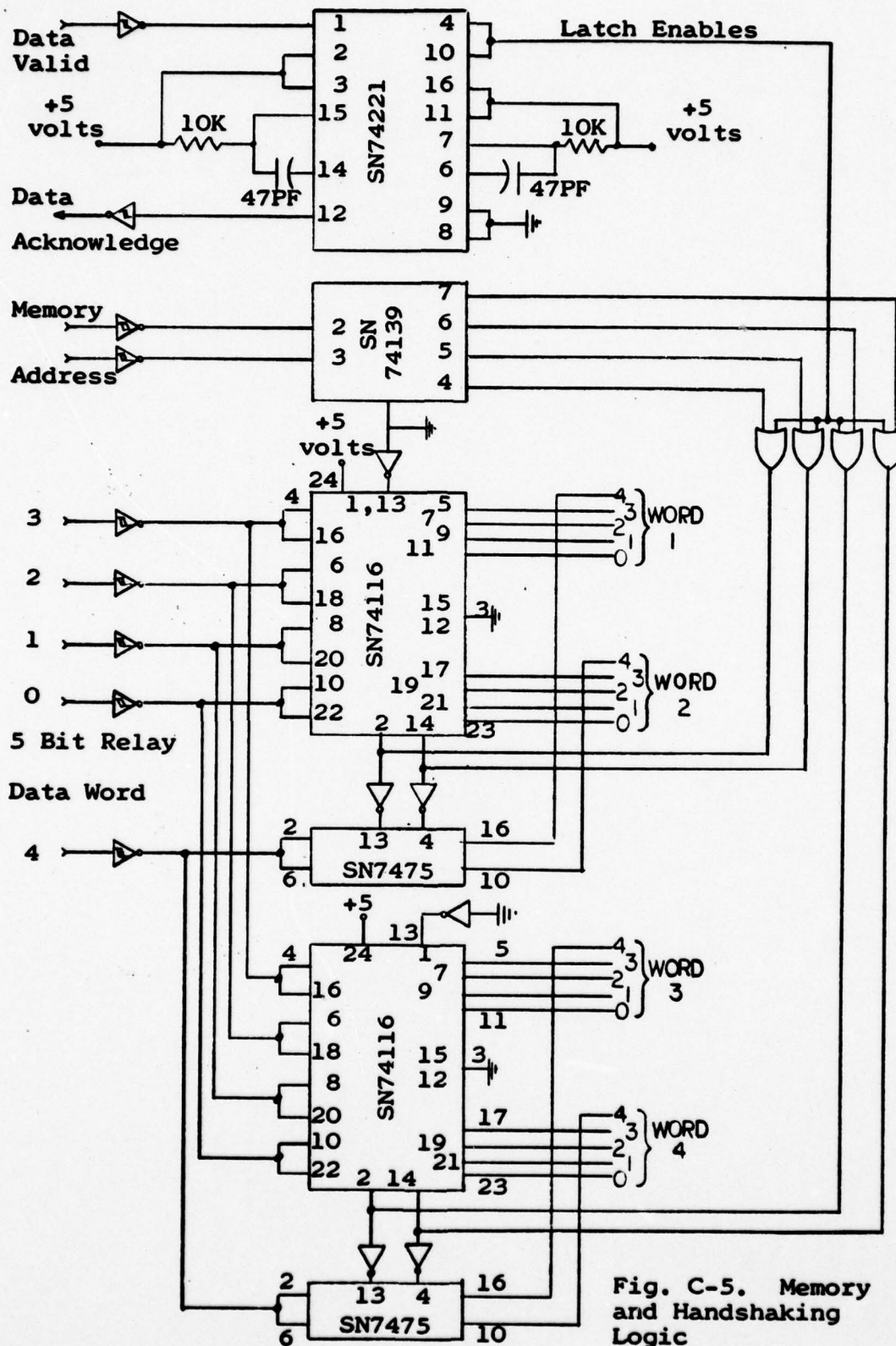


Fig. C-5. Memory and Handshaking Logic

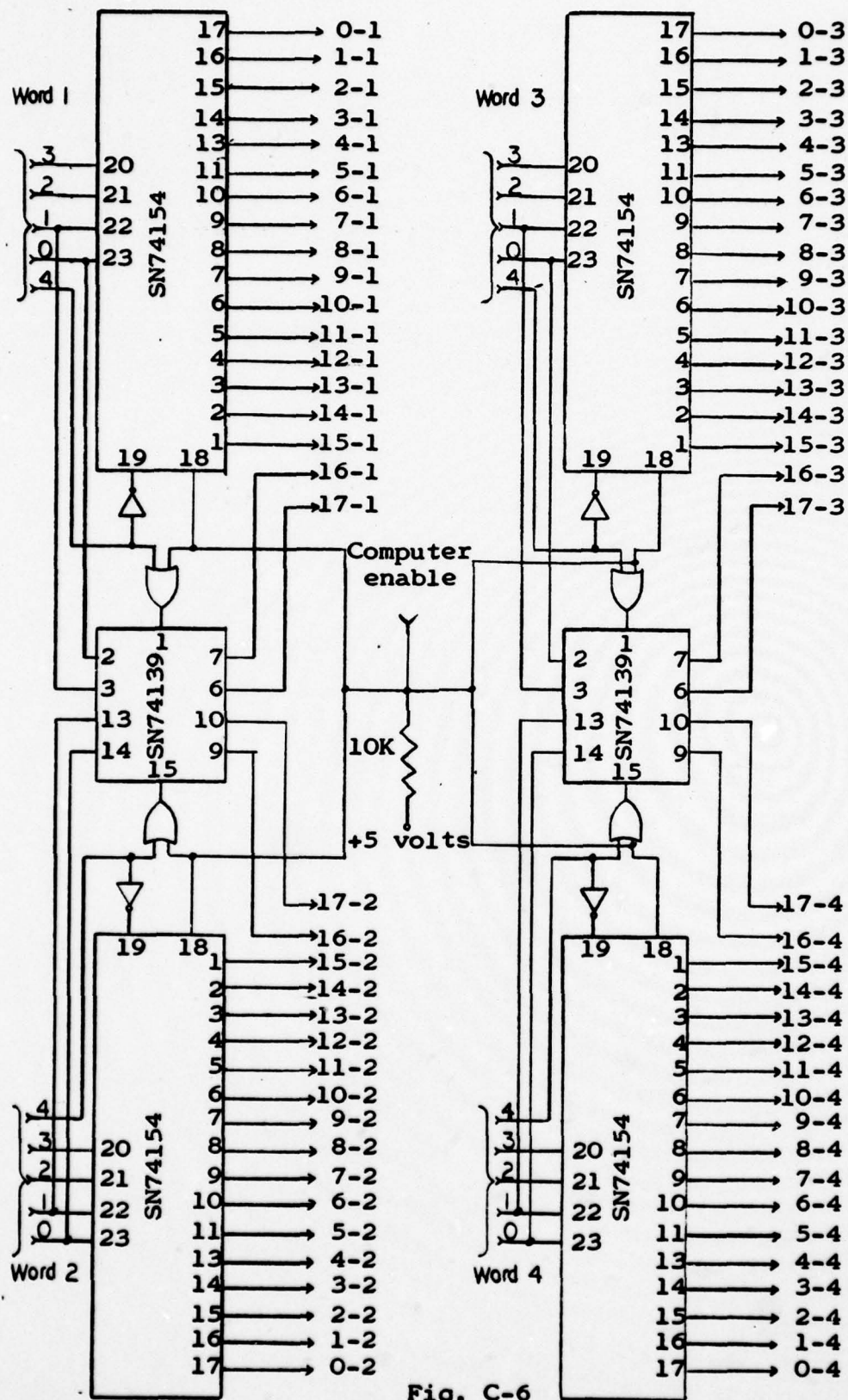
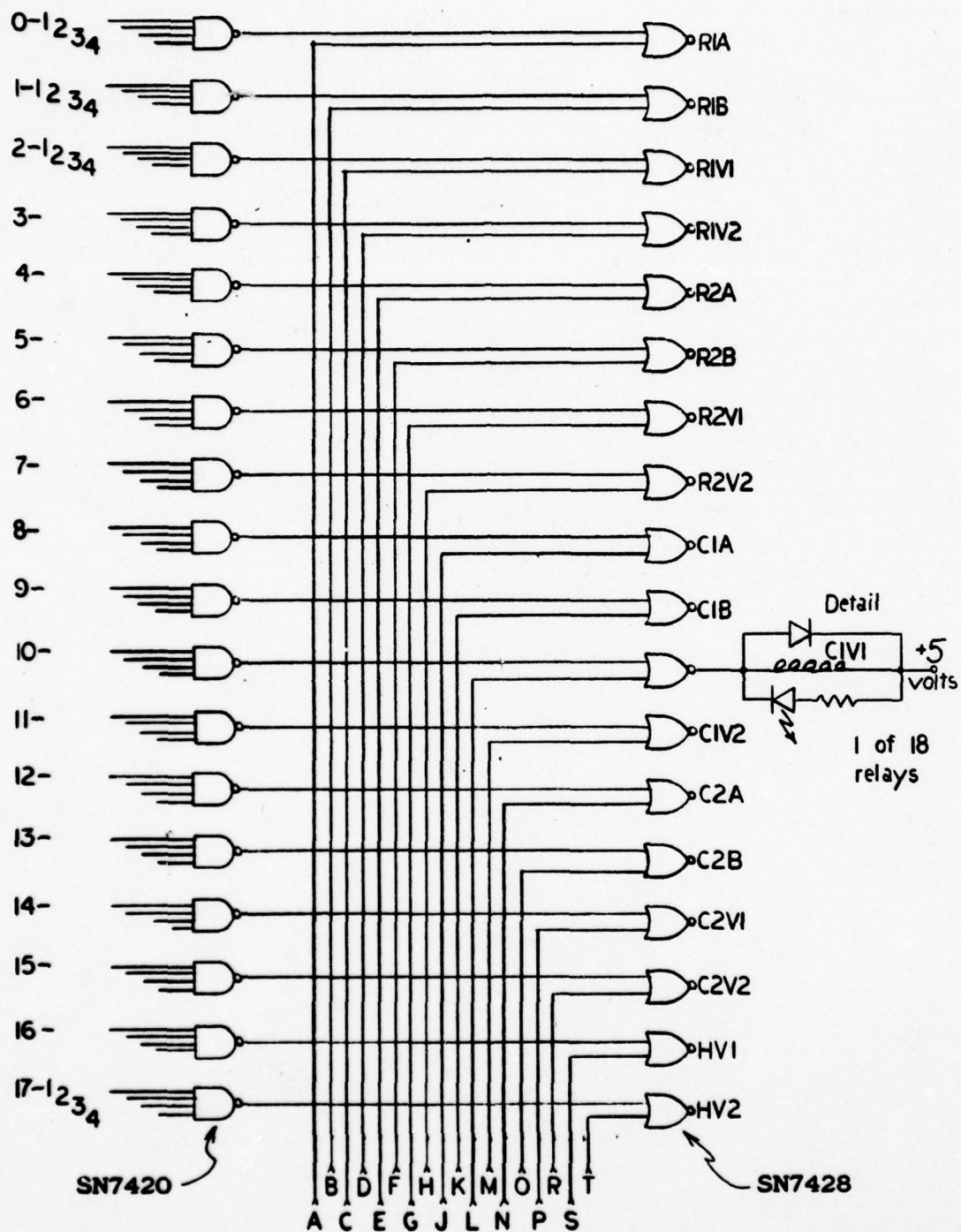


Fig. C-6



Inputs from Manual Control Logic (Fig. C-8)

Fig. C-7. Relay Select Logic and Drivers

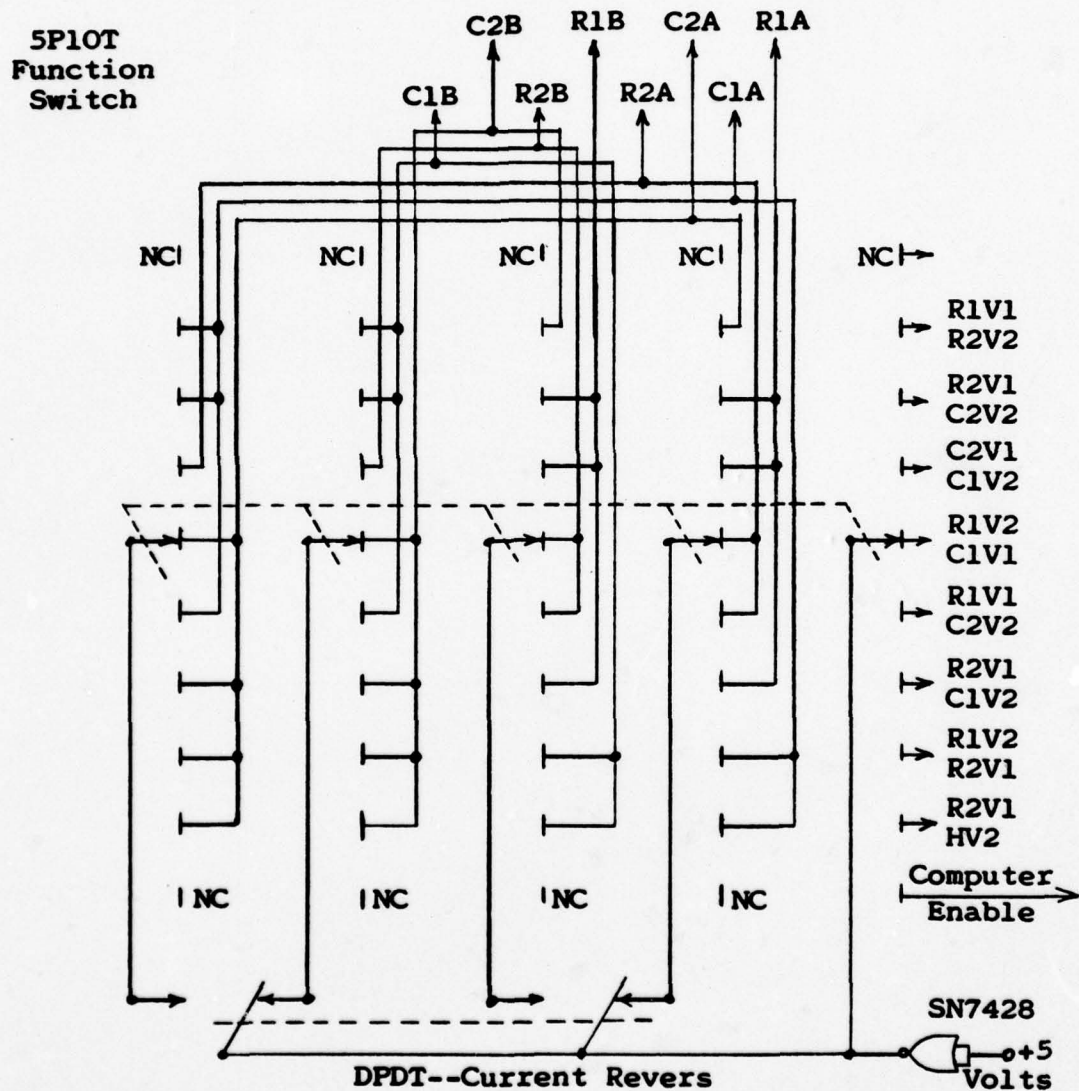
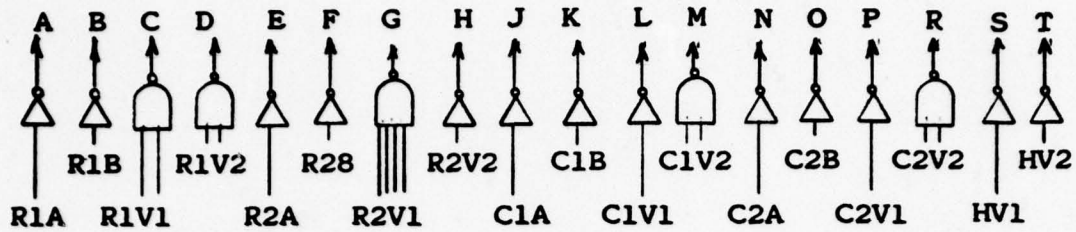


Fig. C-8. Manual Control and Current Reversing Logic

Appendix D

Data indicates the weak-field Hall coefficient plateau, Fig. D-1, is to be measured at magnetic fields less than 100 gauss for temperatures below 50° K and probably less than 50 gauss for temperatures less than 25° K.

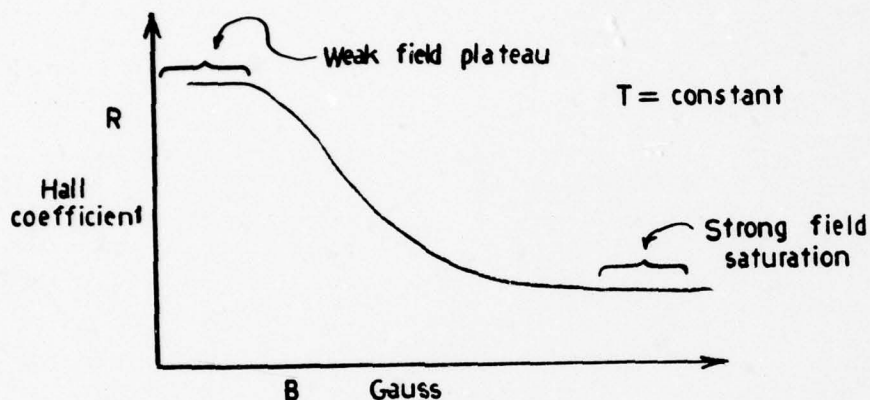


Fig. D-1. Weak and Strong Field Plateau

Changes in Hall and resistivity voltages could not be accurately read at magnetic-field strengths less than 70 gauss at all temperatures. The measuring system noise with sample probes shorted together was measured at 40 microvolts peak to peak. It is in all probability that 1 to 10 microvolt changes in Hall and resistivity voltages are occurring when the magnetic-field strength is varied at strengths less than 100 gauss and thus Hall and resistivity voltages are lost in the noise. Data at slightly stronger magnetic-field intensities tends to support this assumption. At 25° K with the magnetic field changed from 100 gauss to 500 gauss the Hall voltage changed 400 ± 40 microvolts.

The problem of noise also obscured the magnetoresistance weak field to a much greater extent than observed for the Hall coefficient. For temperatures less than 40° K and magnetic fields less than 300 gauss the magnetoresistance error is in excess of 800%. At one kilogauss the error is 1%.

A well-defined strong-field saturation of the Hall coefficient (Fig. D-1) is not present in the data. For temperatures less than 35° K the Hall coefficient decreases as it theoretically should as the magnetic field is increased from the low-field region, but then reverses its trend and begins increasing as B is increased further (Fig. D-2).

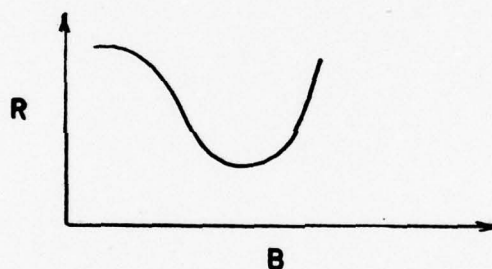


Fig. D-2. Experimental Hall Data for T Less than 35° K

For temperatures greater than 35° K the Hall coefficient shows a plateau region at intermediate B-field values, before continuing to decrease again at higher fields (Fig. D-3).

The Ettingshausen, Nernst, and Righi-Leduc effects were considered as possible explanations. Since these are adiabatic effects and the data voltages did not wander over a period of time after the magnetic field was reversed

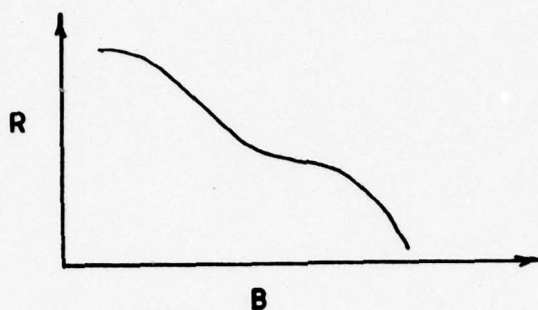


Fig. D-3. Experimental Hall Data for
T Greater than 35° K

through the sample, these types of effects were discounted. Thermoelectric effects such as the Seebeck, Peltier, and Thomson effects again require temperature gradients. The generated voltages would have to be several millivolts to offset the data enough to duplicate the curves we compiled. Sample inhomogeneity is a possible cause; however, time did not permit a literature search for information on this prospect. A great number of possibilities can be eliminated when data can be gathered on more samples. It is an interesting fact that this inflection point in the strong field occurs at increasing field strengths as the temperature increases. Calculations by Dr. Barry Green of the Materials Laboratory show that the inflection point occurs at magnetic-field strengths where theoretically we would expect to see the strong-field saturation of the Hall coefficient. By assuming that the Hall coefficient taken at this inflection point is the value of the Hall coefficient at the limit as the magnetic field approaches infinity, values of the Hall coefficient factor can be calculated that

correspond well with theoretically predicted values (Fig. 13 in Section V). Values for the weak-field Hall coefficient were estimated from the data plotted in this Appendix and Eq (15) was used to calculate the weak-field Hall coefficient factor

$$r_0 = \frac{R_0}{R_\infty} . \quad (15)$$

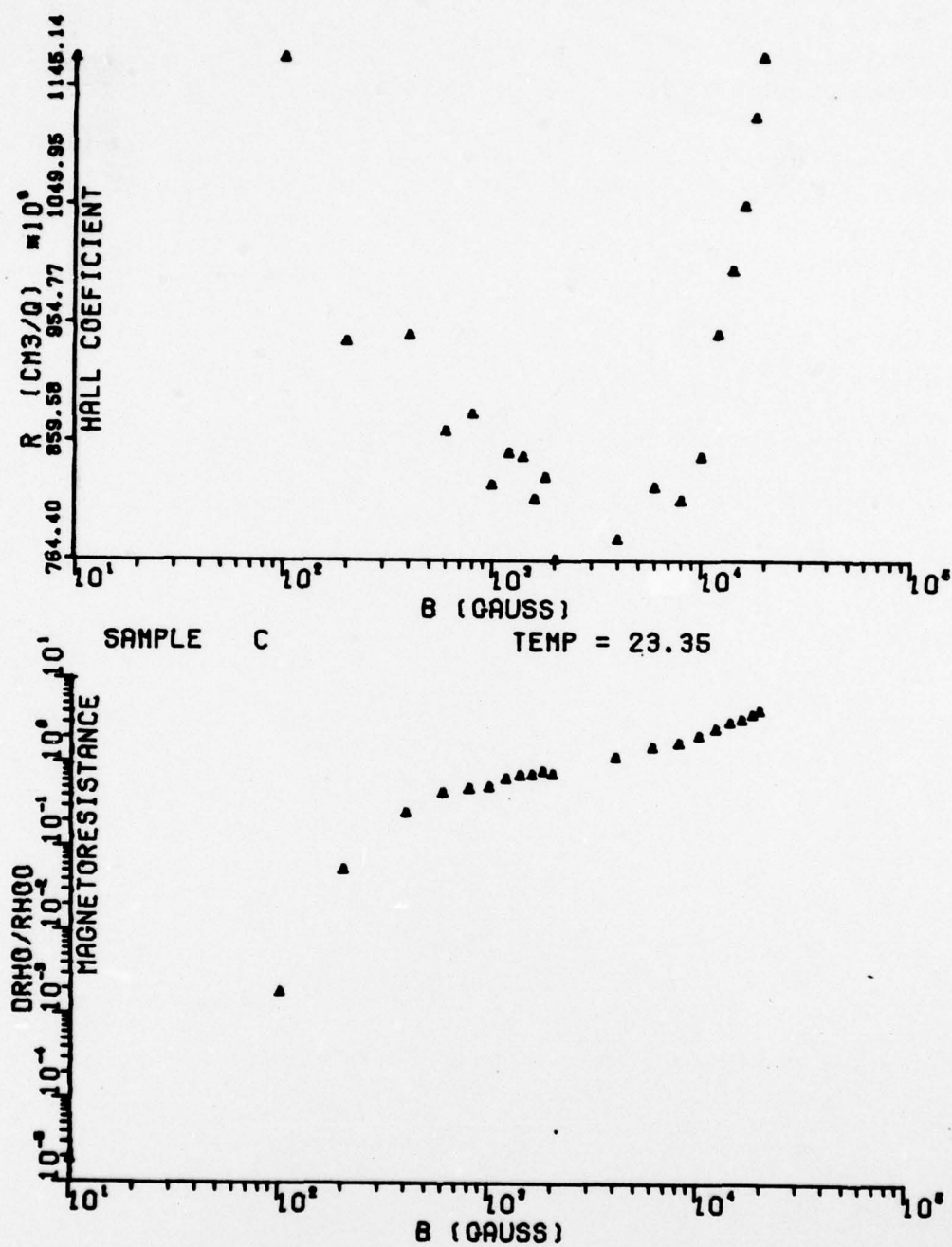
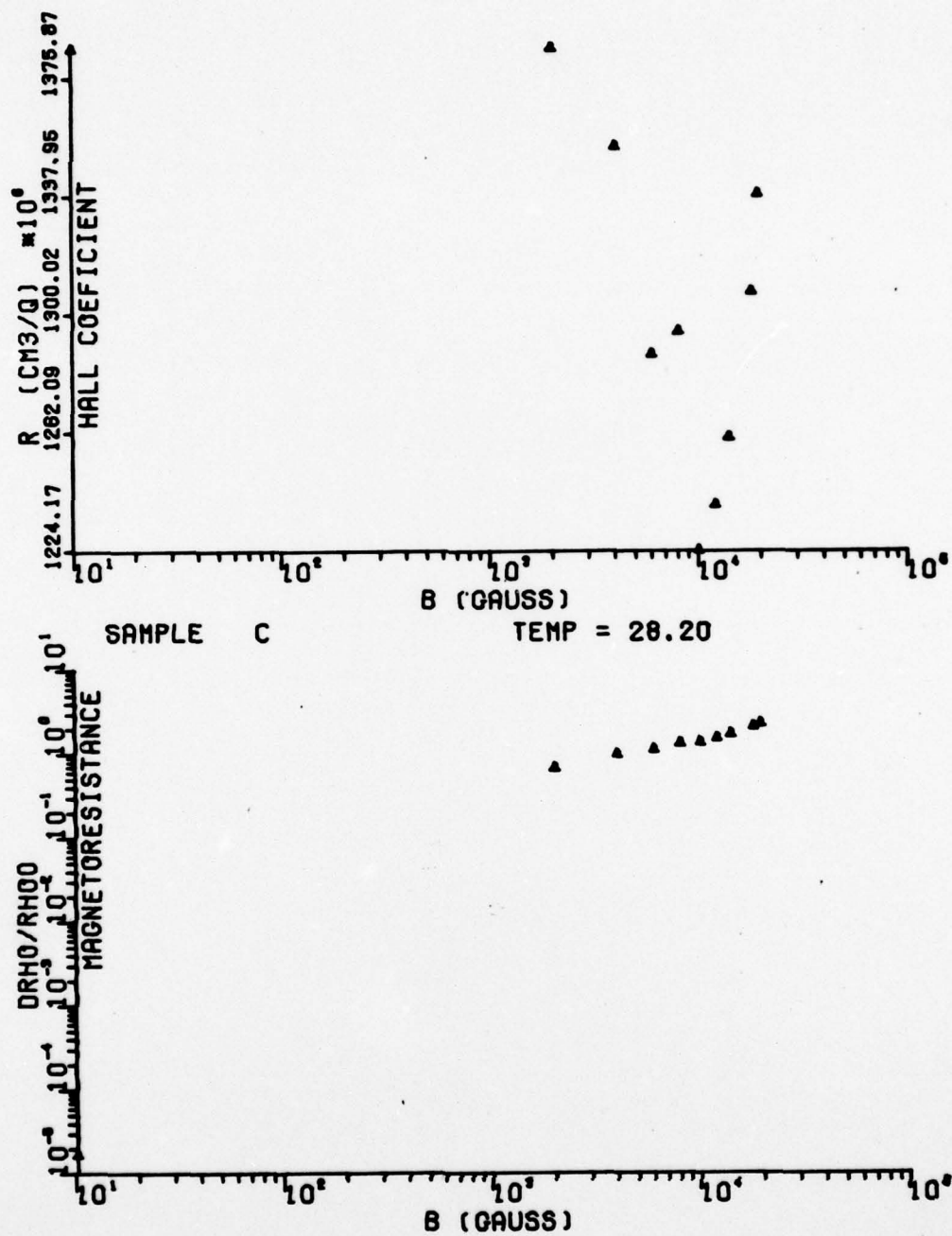


Fig. D-4



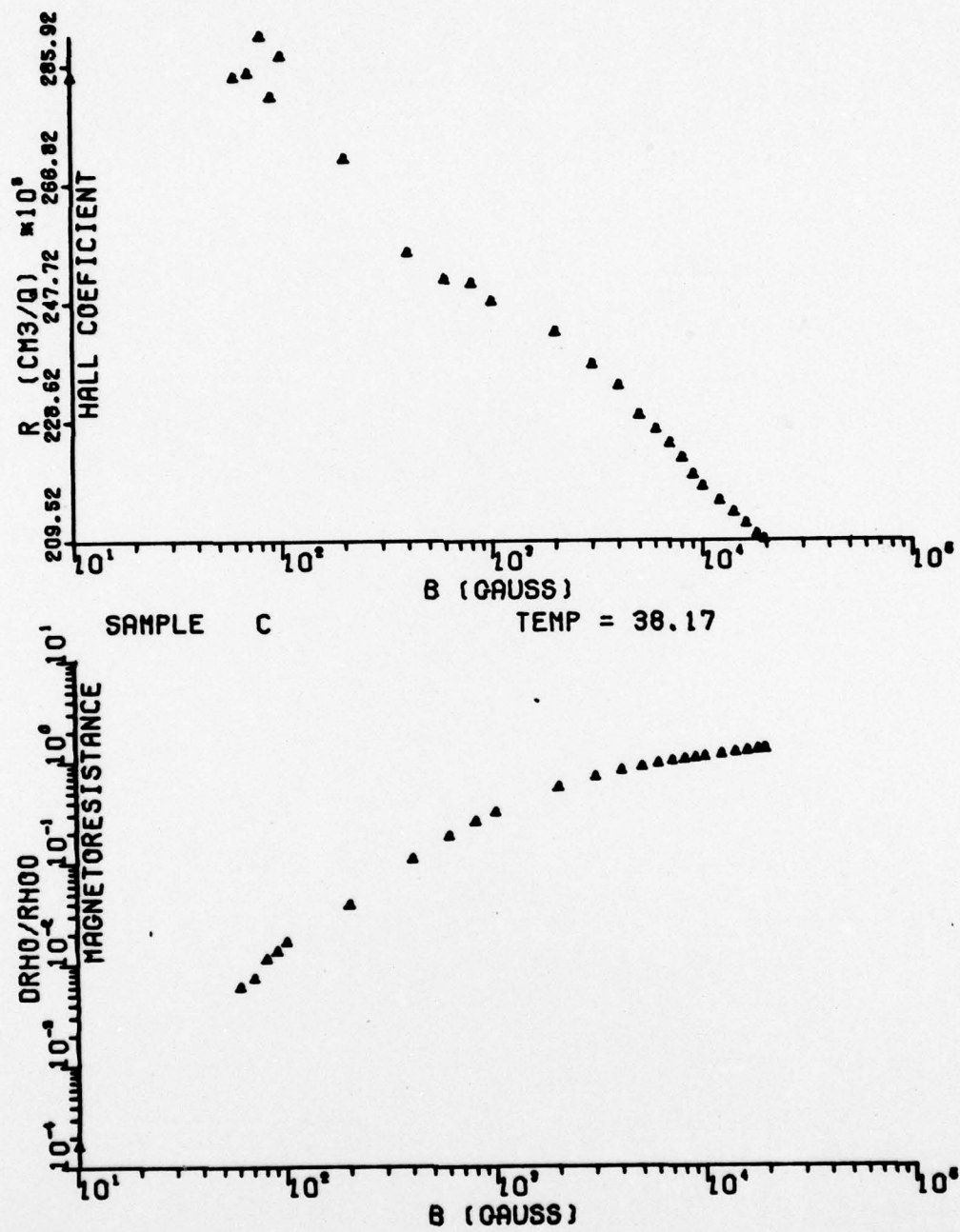


Fig. D-6

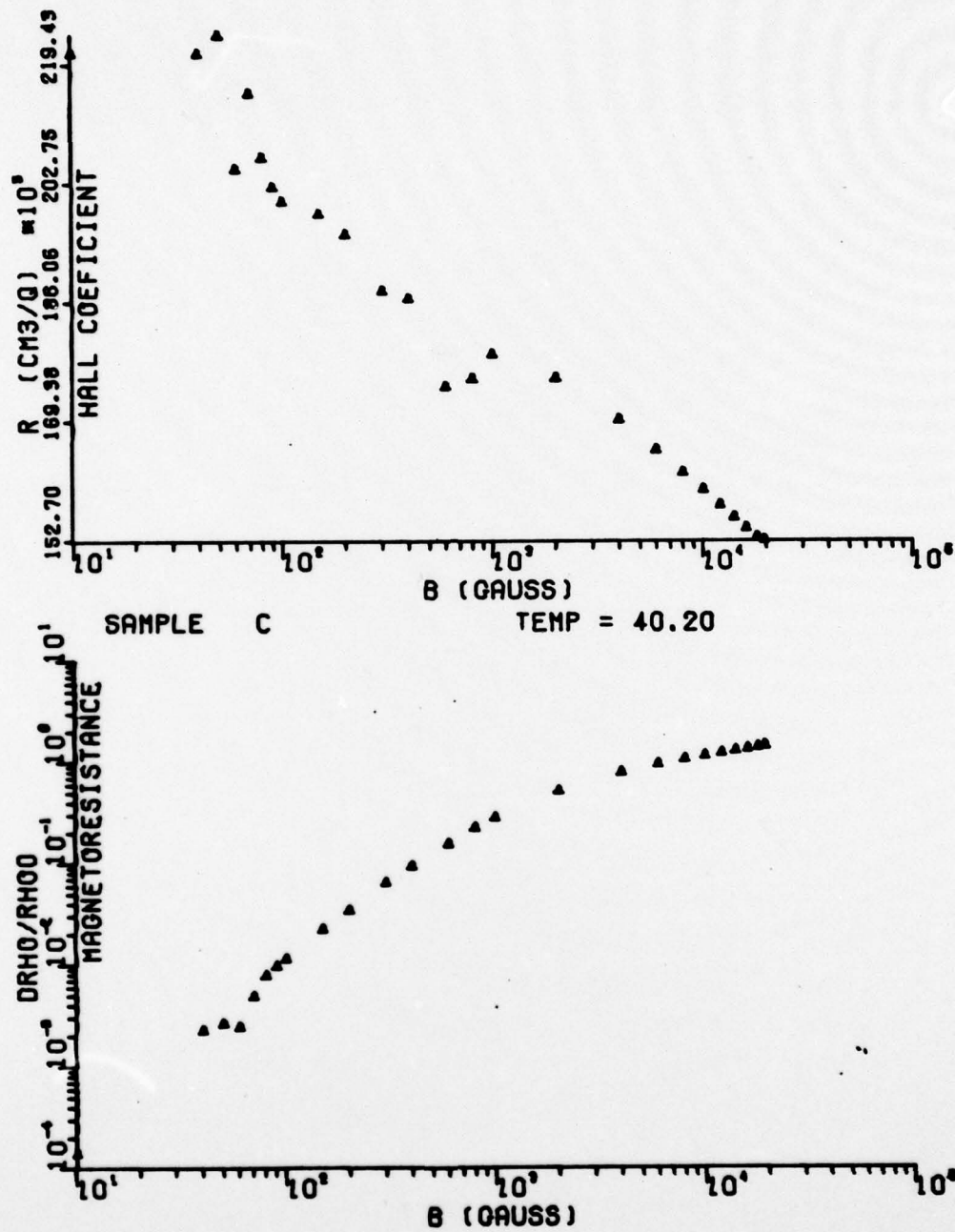


Fig. D-7

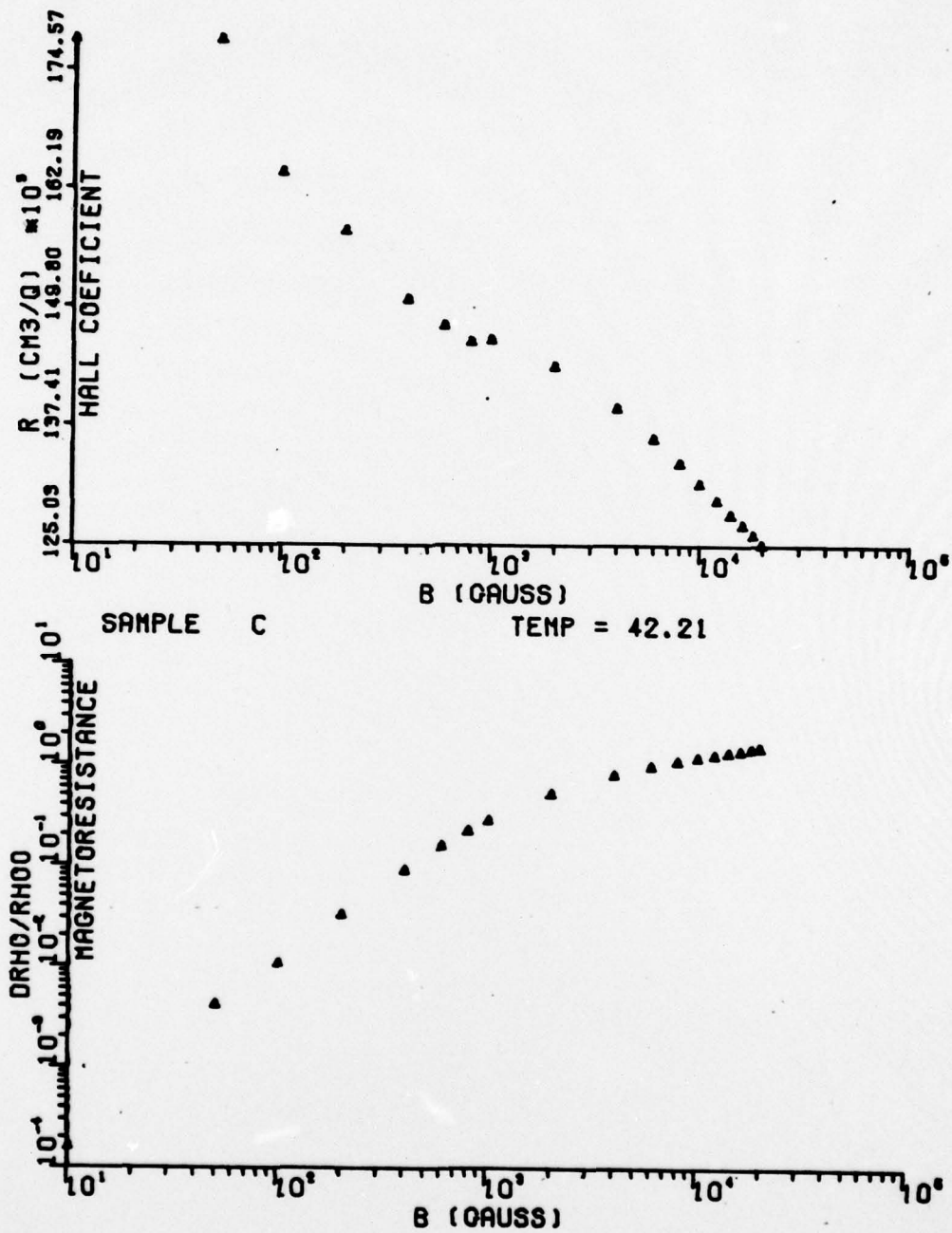


Fig. D-8

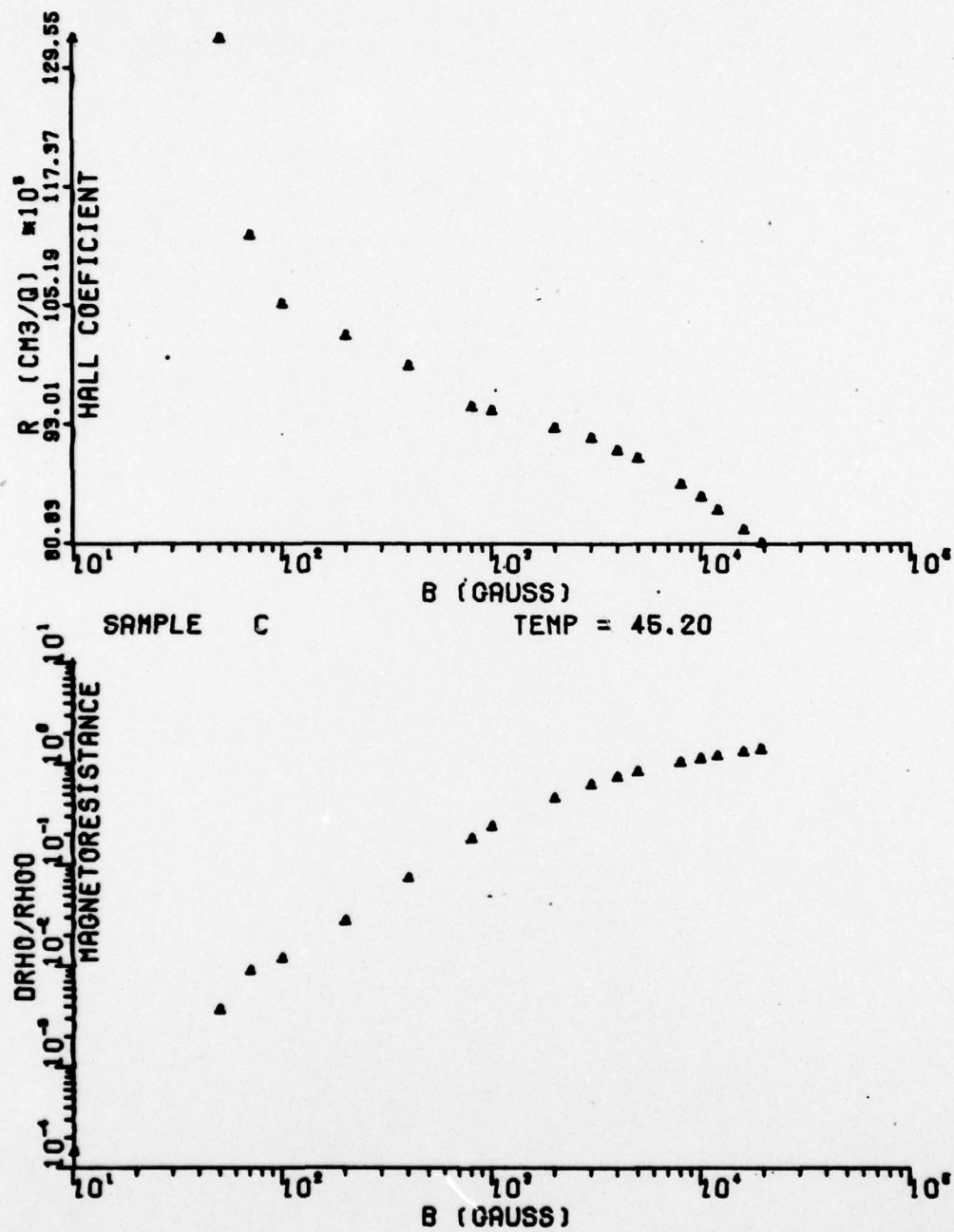


Fig. D-9

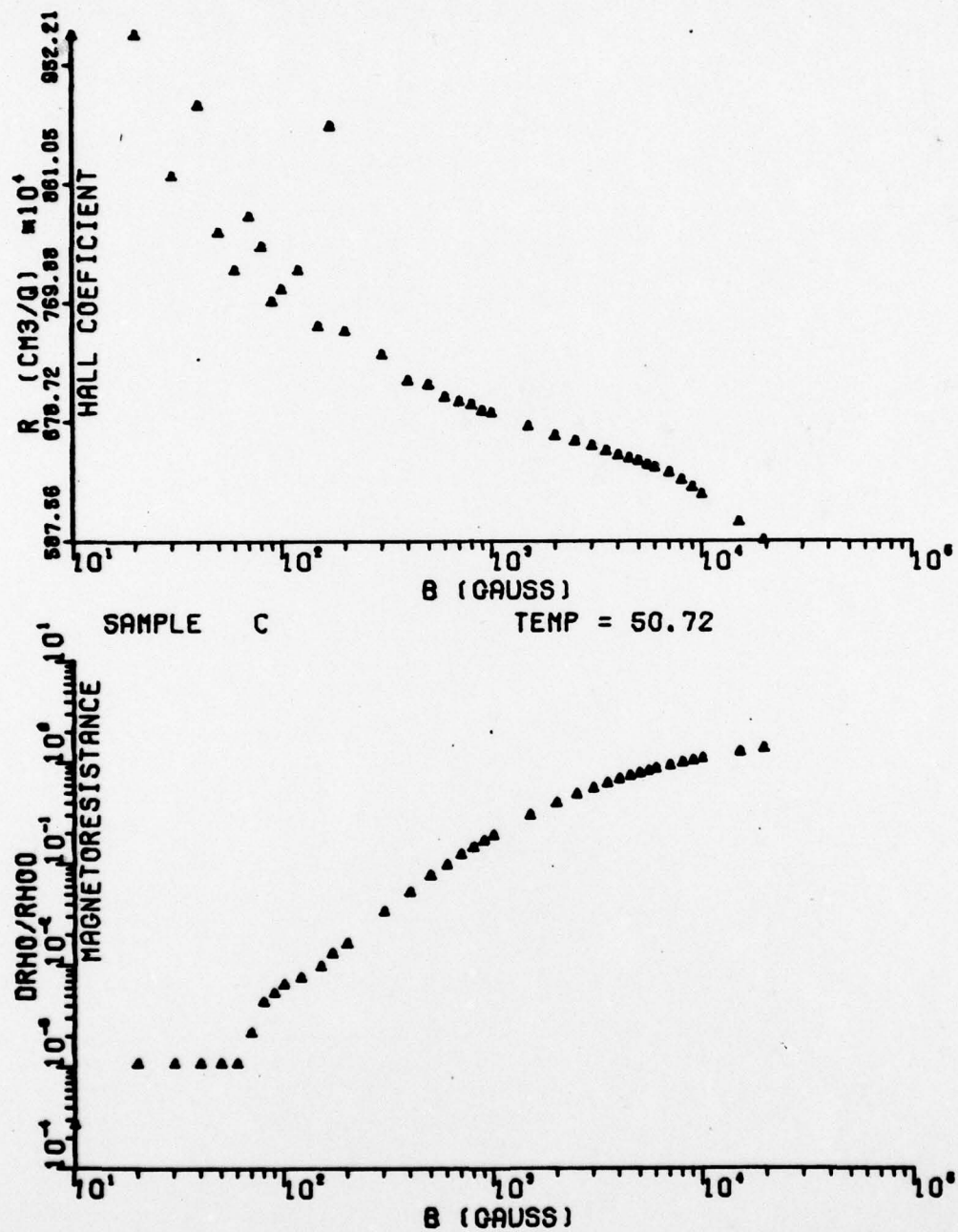


Fig. D-10

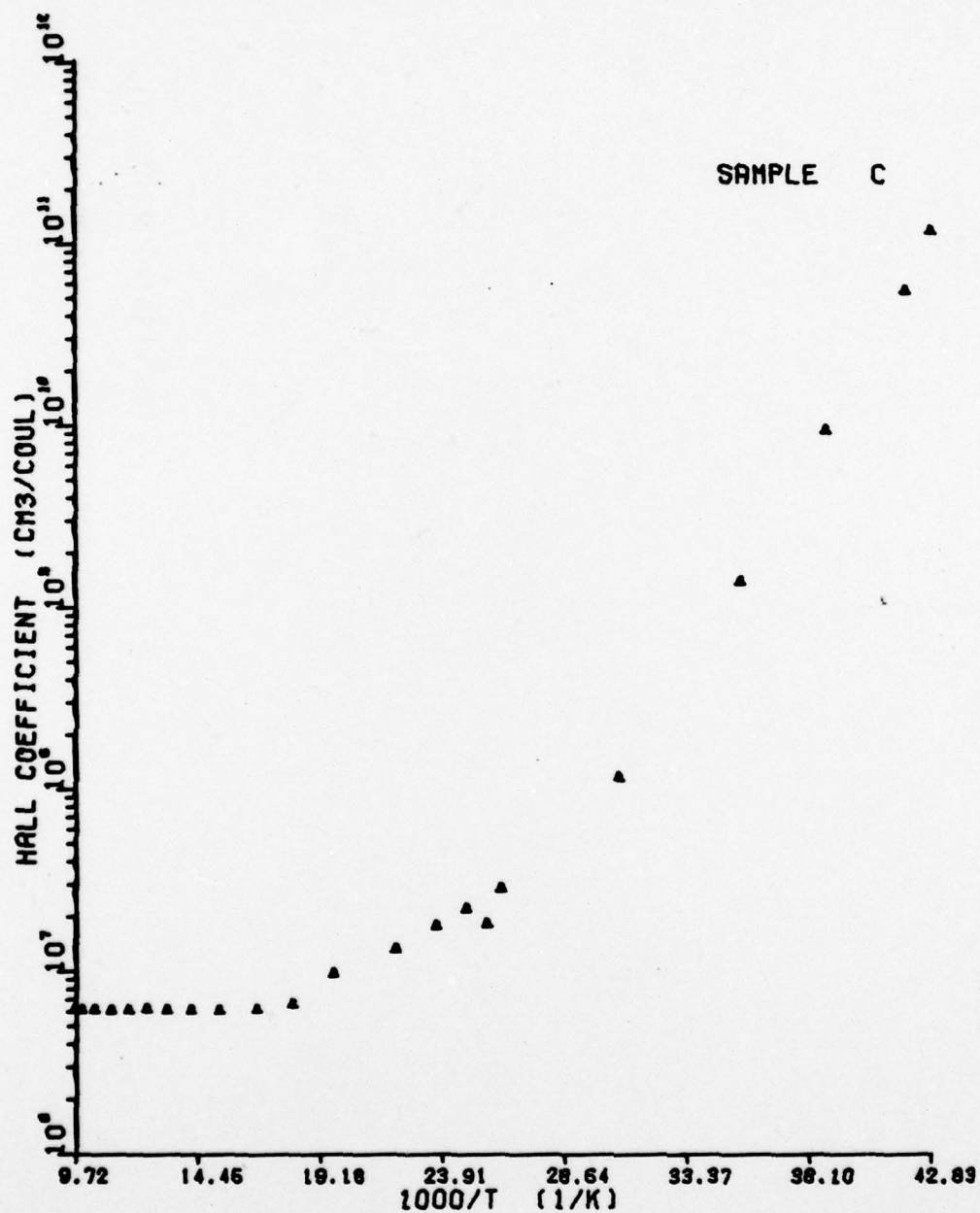


Fig. D-11. Weak-field Hall Coefficient

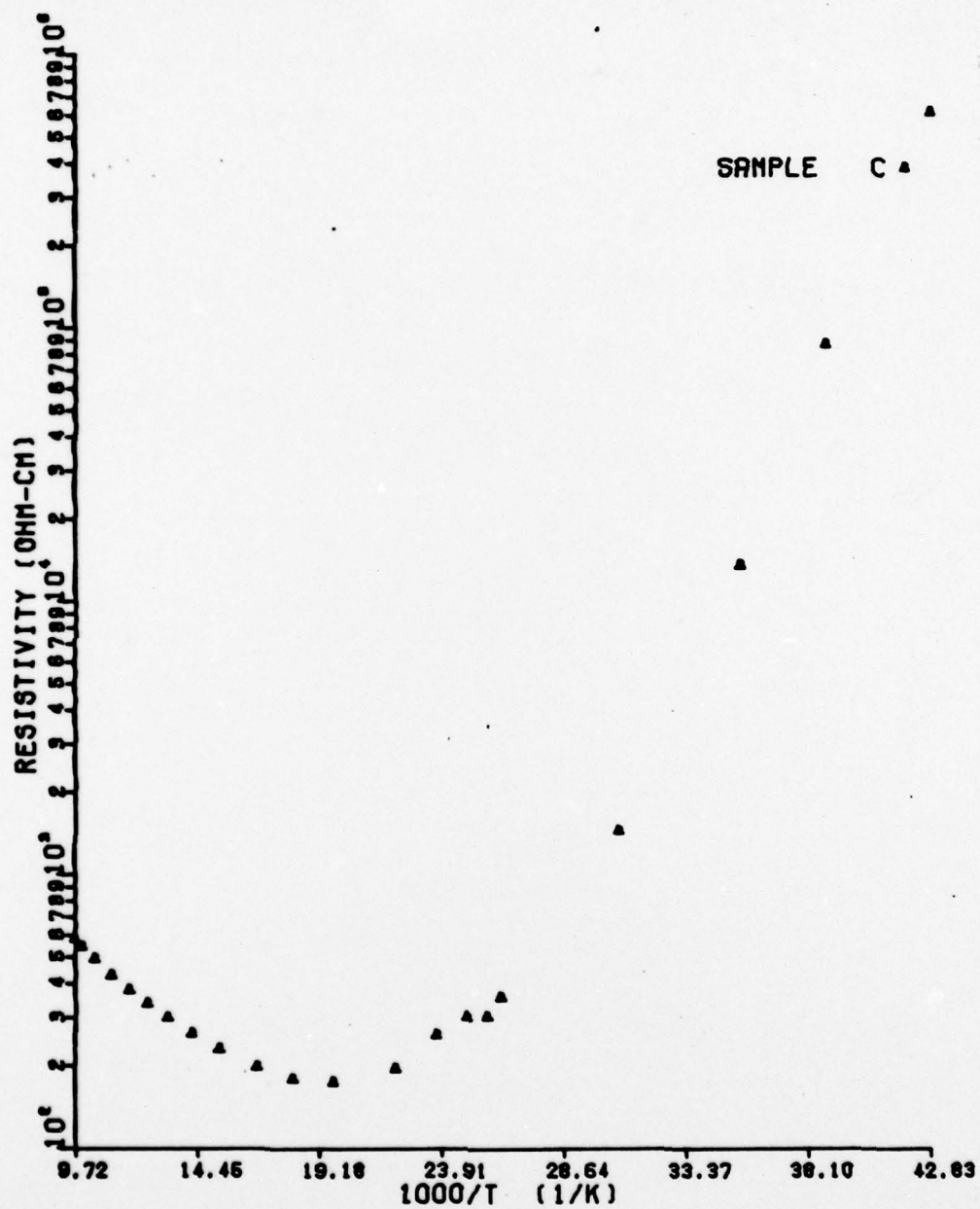


Fig. D-12. Zero-field Resistivity

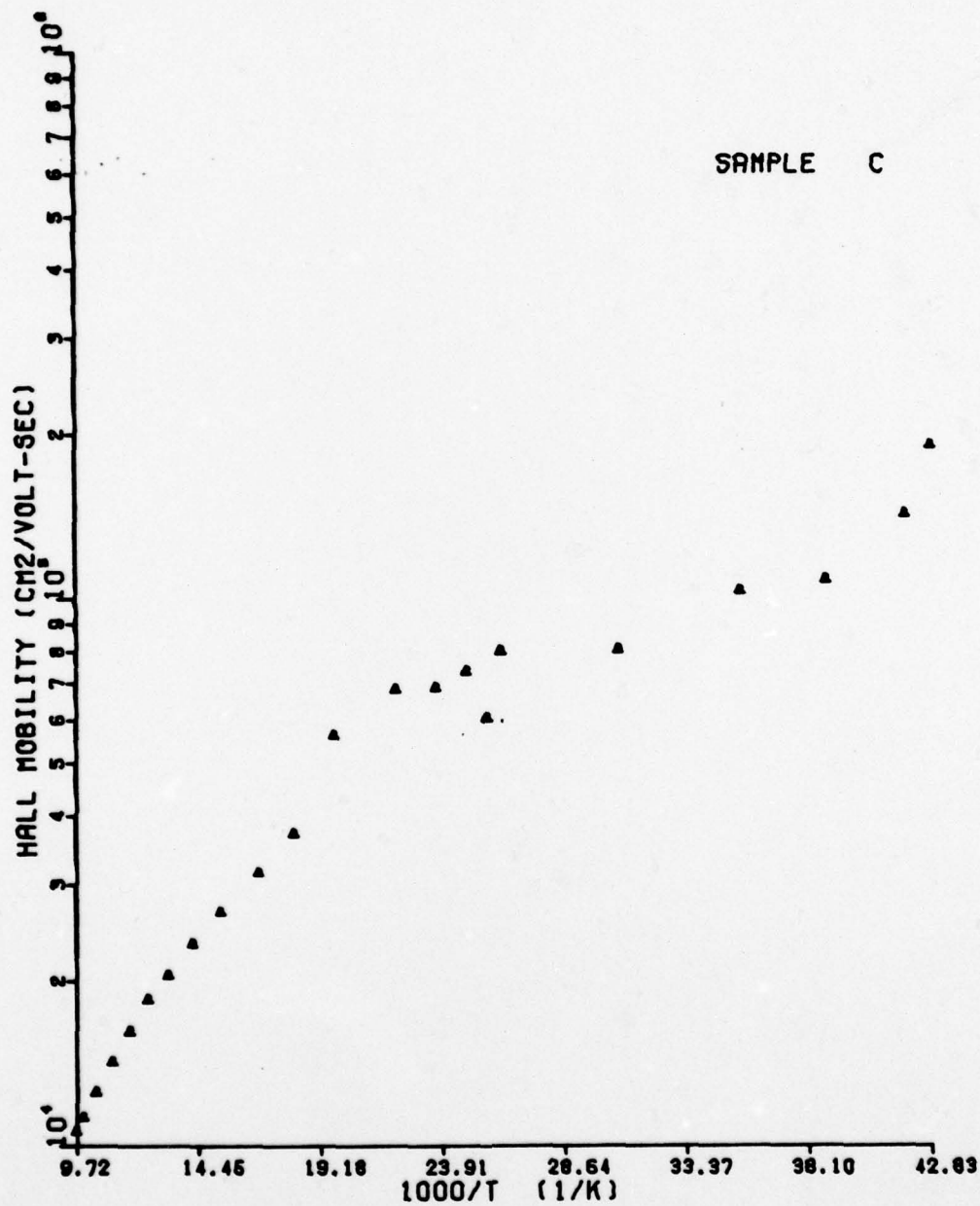


Fig. D-13. Weak-field Hall Mobility

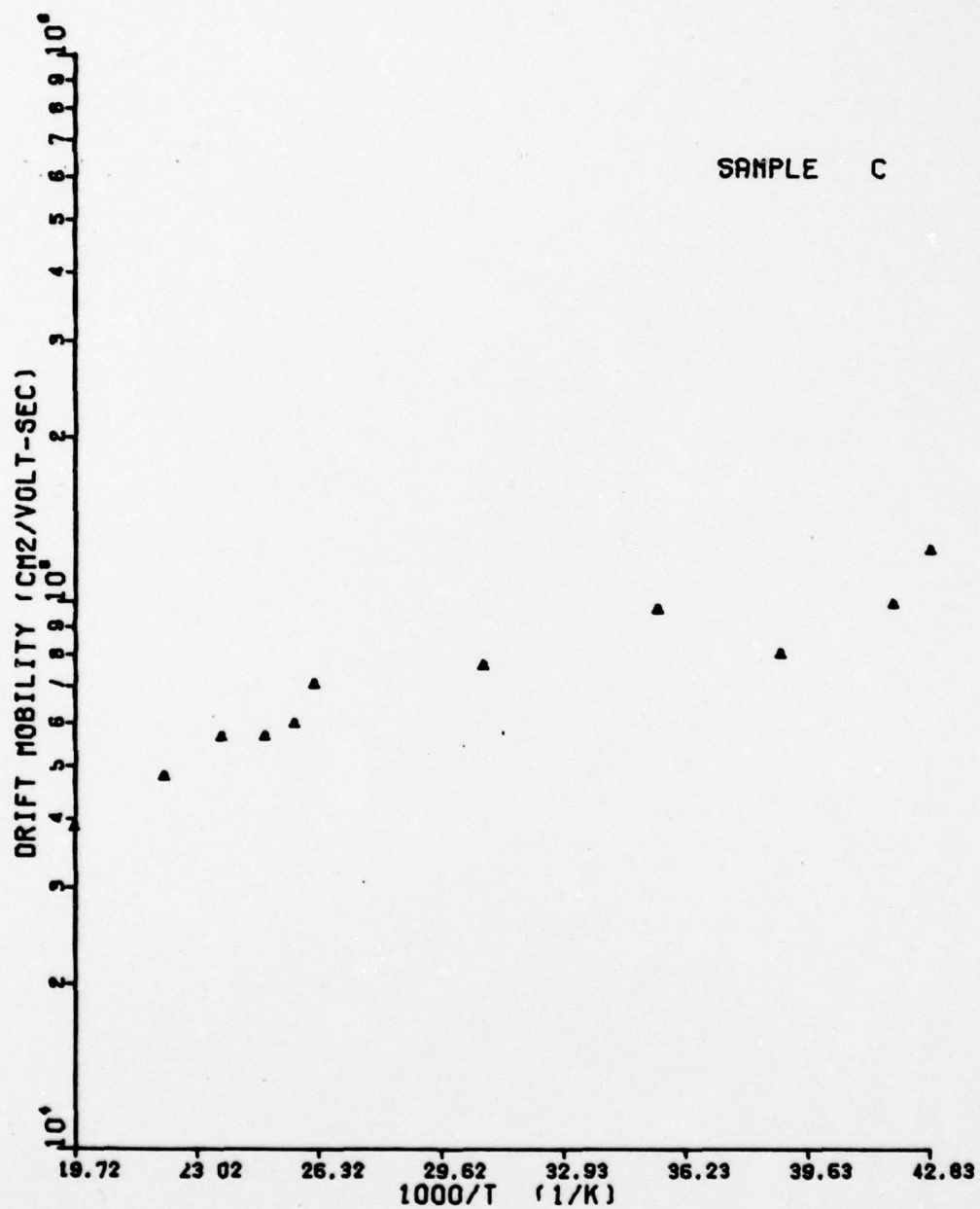


Fig. D-14. Weak-field Drift Mobility

Vita

Robert George Schwein, Jr. was born on 14 September 1946 in Orlando, Florida. He graduated from high school in Alexandria, Virginia in 1964 and attended the University of Cincinnati from which he received the degree of Bachelor of Science Electrical Engineering. Upon graduation, he received a commission in the USAF through the ROTC program. He was employed as an electrical engineer by the Gene Lowe Company, Cincinnati, Ohio until called for active duty in September 1969. He completed pilot training at Reese AFB and received his wings in November 1970. He then served as a forward air controller, piloting OV-10s at Ben Houi, Viet Nam. Upon his return from South East Asia in 1971, he completed a four-year tour as instructor pilot in the Air Training Command at Laughlin AFB, Texas. In June 1976 he entered the School of Engineering, Air Force Institute of Technology.

Permanent address: 121 Joe Rice Drive
Del Rio, Texas 78840

UNCLASSIFIED

SECURITY CLASSIFICATION OF THIS PAGE (When Data Entered)

REPORT DOCUMENTATION PAGE		READ INSTRUCTIONS BEFORE COMPLETING FORM
1. REPORT NUMBER AFIT/GEOPH/78-1	2. GOVT ACCESSION NO. (9) Master's thesis	3. RECIPIENT'S CATALOG NUMBER
4. TITLE (and Subtitle) MAGNETORESISTANCE AND HALL MEASUREMENT OF ULTRA-PURE SILICON.	5. TYPE OF REPORT & PERIOD COVERED M.S. Thesis	
7. AUTHOR(s) Robert W. Schwein, Jr	6. PERFORMING ORG. REPORT NUMBER	
9. PERFORMING ORGANIZATION NAME AND ADDRESS Air Force Institute of Technology (AFIT-EN) Wright-Patterson AFB, Ohio 45433	8. CONTRACT OR GRANT NUMBER(s) (12) 71p	
11. CONTROLLING OFFICE NAME AND ADDRESS Laser and Optical Materials Branch (AFML/LPO) Air Force Materials Laboratory Wright-Patterson AFB, Ohio 45433	10. PROGRAM ELEMENT, PROJECT, TASK AREA & UNIT NUMBERS Project 2306-Q1-02 (16) (17) Q1	
14. MONITORING AGENCY NAME & ADDRESS (if different from Controlling Office)	13. NUMBER OF PAGES 69	
	15. SECURITY CLASS. (of this report)	
	15a. DECLASSIFICATION/DOWNGRADING SCHEDULE	
16. DISTRIBUTION STATEMENT (of this Report) Approved for public release; distribution unlimited		
17. DISTRIBUTION STATEMENT (of the abstract entered in Block 20, if different from Report)		
18. SUPPLEMENTARY NOTES Approved for public release; IAW AFR 190-17 JERRAL F. GUESS, Captain, USAF Director of Information		
19. KEY WORDS (Continue on reverse side if necessary and identify by block number) Silicon Ultra-Pure Hall Effect Magnetoresistance Automation		
20. ABSTRACT (Continue on reverse side if necessary and identify by block number) Experimental equipment was designed and built to allow automated galvanomagnetic data acquisition on semiconductor samples with resistances up to 10^{12} ohms. Hall and magnetoresistance data was taken on one p-type silicon sample with Boron impurity partially compensated by Phosphorus. Data was taken in a temperature range of 23°K to 105°K with magnetic-field strengths up to 20 Kilogauss. Magnetic-field direction was [111] and		

DD FORM 1 JAN 73 1473

EDITION OF 1 NOV 65 IS OBSOLETE

UNCLASSIFIED

SECURITY CLASSIFICATION OF THIS PAGE (When Data Entered)

012 225

Am

UNCLASSIFIED

SECURITY CLASSIFICATION OF THIS PAGE(When Data Entered)

current in the sample was $[1\bar{1}0]$ or equivalent. Results showed that a 40-microvolt noise level in equipment amplifiers obliterated most weak-field data, and possible sample inhomogeneity caused unpredicted strong-field data trends.

The measured total impurity concentration was $2 \times 10^{12} \text{ cm}^{-3}$ and data analyses showed that weak-field measurements must be made with magnetic-field strengths less than 50 gauss for temperatures less than 60°K and strong-field saturation occurs at approximately 2 Kilogauss. The Hall coefficient factor was calculated from the weak- and strong-field data and results approached theoretical values.

UNCLASSIFIED

SECURITY CLASSIFICATION OF THIS PAGE(When Data Entered)